

1 ***Drosophila* nicotinic acetylcholine receptor subunits and their native**
2 **interactions with insecticidal peptide toxins**

3 Dagmara Korona^{1*}, Benedict Dirnberger^{1,2,4*}, Carlo N G Giachello^{4*}, Rayner M L Queiroz²,
4 David-Paul Minde², Michael J Deery², Glynnis Johnson¹, Karin H Müller³, Lucy C Firth⁴,
5 Fergus G Earley⁴, Steven Russell¹ ** and Kathryn S Lilley⁵ **

6

7

8 ¹Department of Genetics, University of Cambridge, Downing Street, Cambridge, CB2 3EH,
9 United Kingdom

10 ²Cambridge Centre for Proteomics, Department of Biochemistry, Gleeson Building,
11 University of Cambridge, Tennis Court Road, Cambridge, CB2 1GA, United Kingdom

12 ³Cambridge Advanced Imaging Centre, Department of Physiology, Development and
13 Neuroscience/Anatomy Building, University of Cambridge, Downing Street, CB2 3DY,
14 United Kingdom

15 ⁴Syngenta, Jealott's Hill International Research Centre, Bracknell, RG42 6EY, United
16 Kingdom

17 ⁵Cambridge Centre for Proteomics, Department of Biochemistry, Gleeson Building,
18 University of Cambridge, Tennis Court Road, Cambridge, CB2 1GA, United Kingdom.
19 k.s.lilley@bioc.cam.ac.uk

20 *These authors contributed equally: Dagmara Korona, Benedict Dirnberger, Carlo N G
21 Giachello

22 **Correspondence should be addressed to Kathryn S Lilley k.s.lilley@bioc.cam.ac.uk and
23 Steven Russell sr120@cam.ac.uk

24

25

26

27

28 **Abstract**

29 *Drosophila* nicotinic acetylcholine receptors (nAChRs) are ligand-gated ion channels that
30 represent a target for insecticides. Peptide neurotoxins are known to block nAChRs by binding
31 to their target subunits, however, a better understanding of receptor subunit composition is
32 needed for effective design of insecticides. To facilitate the analysis of nAChRs we used a
33 CRISPR/Cas9 strategy to generate null alleles for all ten *nAChR* subunit genes in a common
34 genetic background. We studied interactions of nAChR subunits with peptide neurotoxins by
35 larval injections and styrene maleic acid lipid particles (SMALPs) pull-down assays. For the
36 null alleles we determined the effects of α -Bungarotoxin (α -Btx) and ω -Hexatoxin-Hv1a
37 (Hv1a) administration, identifying potential receptor subunits implicated in the binding of these
38 toxins. We employed pull-down assays to confirm α -Btx interactions with the $D\alpha 5$, $D\alpha 6$, $D\alpha 7$
39 subunits. Finally, we report the localization of fluorescent tagged endogenous $D\alpha 6$ during
40 nervous system development. Taken together this study elucidates native *Drosophila* nAChR
41 subunit interactions with insecticidal peptide toxins and provides a resource for the *in vivo*
42 analysis of insect nAChRs.

43

44

45

46

47

48

49

50

51

52

53

54

55 Introduction

56 Global climate change and other factors are placing increasing demands on available
57 agricultural land to deliver efficient, reliable and sustainable food production. Insecticides are
58 important tools in securing yields of all major crops but need to be continually replaced to
59 overcome resistance in target species and reduce environmental impacts. In addition, new
60 insecticides must have low toxicity to non-target species, particularly the major pollinators
61 essential for agriculture. A large class of insecticide targets are neurotransmitter receptors such
62 as the nicotinic acetylcholine receptors (nAChRs) located in synaptic plasma membranes (Ihara
63 et al., 2020). These pentameric cys-loop ligand-gated ion channels consist of either only α -
64 subunits or α - and β -subunits, with ligand binding sites located between two α -subunits or
65 between α - and β -subunits. Most insect genomes, including that of the highly tractable
66 *Drosophila melanogaster* model, harbour ten highly conserved subunit genes that assemble in
67 various combinations to form the active receptors.

68 An essential pre-requisite for effective design of new insecticides targeting these receptors is
69 understanding the subunit composition of nAChRs and their distinctive binding properties. For
70 many reasons, including low expression in endogenous tissues or difficulties in expressing
71 insect receptors in heterologous systems, the characterisation of functional insect receptors has
72 been challenging (Perry et al., 2021; Zuo et al., 2021; Salgado, 2021). Even in the tractable *D.*
73 *melanogaster* insect model, there has been no systematic isolation of mutations in *nAChR*
74 subunit genes, until recently, when Perry and colleagues described the generation of a new set
75 of null mutations in nine out of the ten *D. melanogaster* subunit genes (Perry et al., 2021).
76 These mutations, however, were generated in different genetic backgrounds necessitating
77 additional work to assay background sensitive phenotypes such as neural or behavioural
78 defects.

79 Several classes of insecticide, the most effective being those in the neonicotinoid and spinosad
80 class, have been shown to bind insect nAChRs highly selectively to block their functions
81 (Chambers et al., 2019; Houchat et al., 2019). Recently, the binding affinity and the positive
82 allosteric effects of ω -Hexatoxin-Hv1a (Hv1a) peptide on nAChRs has been demonstrated
83 (Chambers et al., 2019) and this spider venom peptide is well known for its insecticidal effects.
84 In addition, other peptide toxins, such the snake venom constituent, α -Bungarotoxin (α -Btx),
85 have been widely used to probe nAChR functions, however whether α -Btx harbours a selective
86 insecticidal property is currently unknown. Alpha-Btx is a 74 amino acid peptide that binds

87 irreversibly to nAChR α -subunits in different species, including *D. melanogaster*, although the
88 exact subunit composition of target receptors is not fully understood (Schmidt-Nielsen et al.,
89 1977; Dellisanti et al., 2007; Dacosta et al., 2015). Lansdell and co-workers have shown
90 binding of α -Btx to *D. melanogaster* Da5, Da6, and Da7 subunits in a heterologous S2 cell
91 expression system (Lansdell & Millar, 2004; Lansdell et al., 2012) and the amino acid sequence
92 of these subunits show strong similarity across their ligand-binding domains (LBD).

93 The lipid bilayer surrounding nAChRs is known to be essential for structural integrity, stability
94 and ligand binding (Dacosta et al., 2013). However, this lipid requirement can make analysis
95 of membrane protein complexes challenging. The development of methods for extracting
96 membrane proteins from lipid bilayers using detergents and introducing them into artificial
97 lipid nanodiscs has facilitated a much better characterisation of receptor-ligand interactions
98 (Denisov & Sligar, 2016). The use of detergents generally used to solubilize membrane
99 proteins, however, leads to destabilisation, aggregation and misfolding and are therefore not
100 compatible with this type of analysis (Loo et al., 1996). Styrene maleic acid lipid particles
101 (SMALPs) allow detergent-free extraction of membrane proteins in their local lipid
102 environment and provide a promising technique for investigating receptor-ligand interactions
103 under native conditions (Lee et al., 2016). This is particularly important since loss of lipids
104 surrounding membrane proteins can lead to changes in measured binding affinities (Martens et
105 al., 2018; Gault et al., 2020). The combination of detergent free SMALPs extraction coupled
106 with mass spectrometry analysis provides a potential route for characterising native membrane
107 receptor complexes (Sobotzki et al., 2018; Kalxdorf et al., 2021).

108 Here we report the results from a combined genetic and biochemical analysis of *D.*
109 *melanogaster* nAChRs *in vivo*. Using CRISPR/Cas9 genome engineering we generated new
110 null mutations for all ten receptor subunit genes in a uniform genetic background as well as
111 introducing a fluorescent protein tag into the *nAChRa6* locus. We show that the null mutants
112 in all seven α -subunit genes and two of the three β -subunit genes are viable and fertile, although
113 we find mild morphological defects and some neurological impairment. Mutation of the
114 remaining subunit gene, *nAChR β 1*, is recessive lethal. All nine of the viable null mutants were
115 used to demonstrate a novel selective insecticidal effect of α -Btx on the *nAChRa5*, *nAChRa6*
116 and *nAChRa7* subunits. We also applied the insecticidal Hv1a peptide to the viable null
117 mutants, showing resistance with two subunit gene mutants: *nAChRa4* and *nAChR β 2*. In our
118 biochemical studies we analysed receptor-ligand interactions in native conditions using
119 SMALPs to verify the *in vivo* receptor subunit composition of the α -Btx binding target in adult

120 neural tissue from wild-type and receptor subunit mutants. Our analysis revealed binding of α -
121 Btx to receptors containing $\alpha 5$, $\alpha 6$ and $\alpha 7$ subunits with the analysis of mutants in these
122 subunits genes indicating heterogeneity in α -Btx binding nAChRs. Furthermore, we have
123 identified specific glycosylation sites in $\alpha 5$ and $\alpha 7$ subunits which are known from other
124 studies to play a critical role in α -Btx binding affinity (Dellisanti et al., 2007; Rahman et al.,
125 2020). Localization studies with the $\alpha 6$ subunit tagged at the endogenous locus with a
126 fluorescent reporter shows expression at different developmental stages in specific neuronal
127 cells, including the Kenyon cells of the mushroom bodies, a known site of α -Btx-binding.

128 Results

129 New *D. melanogaster* nicotinic acetylcholine receptor subunit gene mutations

130 To investigate the role of individual nAChR subunits we used CRISPR/Cas9 to generate
131 deletion mutations in each of the seven α -subunit and three β -subunit genes. All of the
132 mutations were generated in virtually identical genetic backgrounds using nanos-Cas9 sources
133 on the second or third chromosome of otherwise genetically homogeneous fly lines. In brief,
134 for each gene we targeted exons shared between all predicted isoforms, close to the N-terminus
135 of the protein. In order to disrupt each coding sequence and facilitate screening we introduced
136 a visible fluorescent marker, DsRED under control of the eye-specific 3xP3 promoter at the
137 targeted locus. Positive lines were confirmed by PCR and sequencing, and subsequently the
138 DsRED marker was excised from the genome by Cre-Lox recombination.

139 For nine out of ten subunit genes we established homozygous viable and fertile stocks, the
140 exception was the *nAChR β 1* gene which proved to be recessive lethal. Although all the other
141 lines are viable, we noticed that most of the mutants, but particularly *nAChR α 1*, *nAChR α 2*,
142 *nAChR α 5* and *nAChR β 3*, exhibited a curled abdomen phenotype that is most prominent in
143 males (approximately 25, 20, 15 and 15 % respectively, Figure 1A). It is possible that this
144 phenotype is a result of defects in neural control of abdominal muscles and it is interesting to
145 note that a previous analysis of an *nAChR α 1* allele reports reduced male courtship and mating
146 (Somers et al., 2017). Since nAChRs are mostly found in the nervous system, we carried out
147 basic climbing assays on the null alleles to assess potential locomotor defects (Figure 1B,
148 Appendix-table 1). We saw little or no impact on the locomotor activity of ten day old flies
149 with *nAChR α 4*, *nAChR α 5*, *nAChR α 7*, *nAChR β 2* or *nAChR β 3* homozygous mutants, however,
150 deletions of *nAChR α 1*, *nAChR α 2* and *nAChR α 6* showed 50-60 % reductions in climbing ability

151 compared to wild-type. In addition, the *nAChRa3* null mutant and heterozygotes for *nAChR β 1*

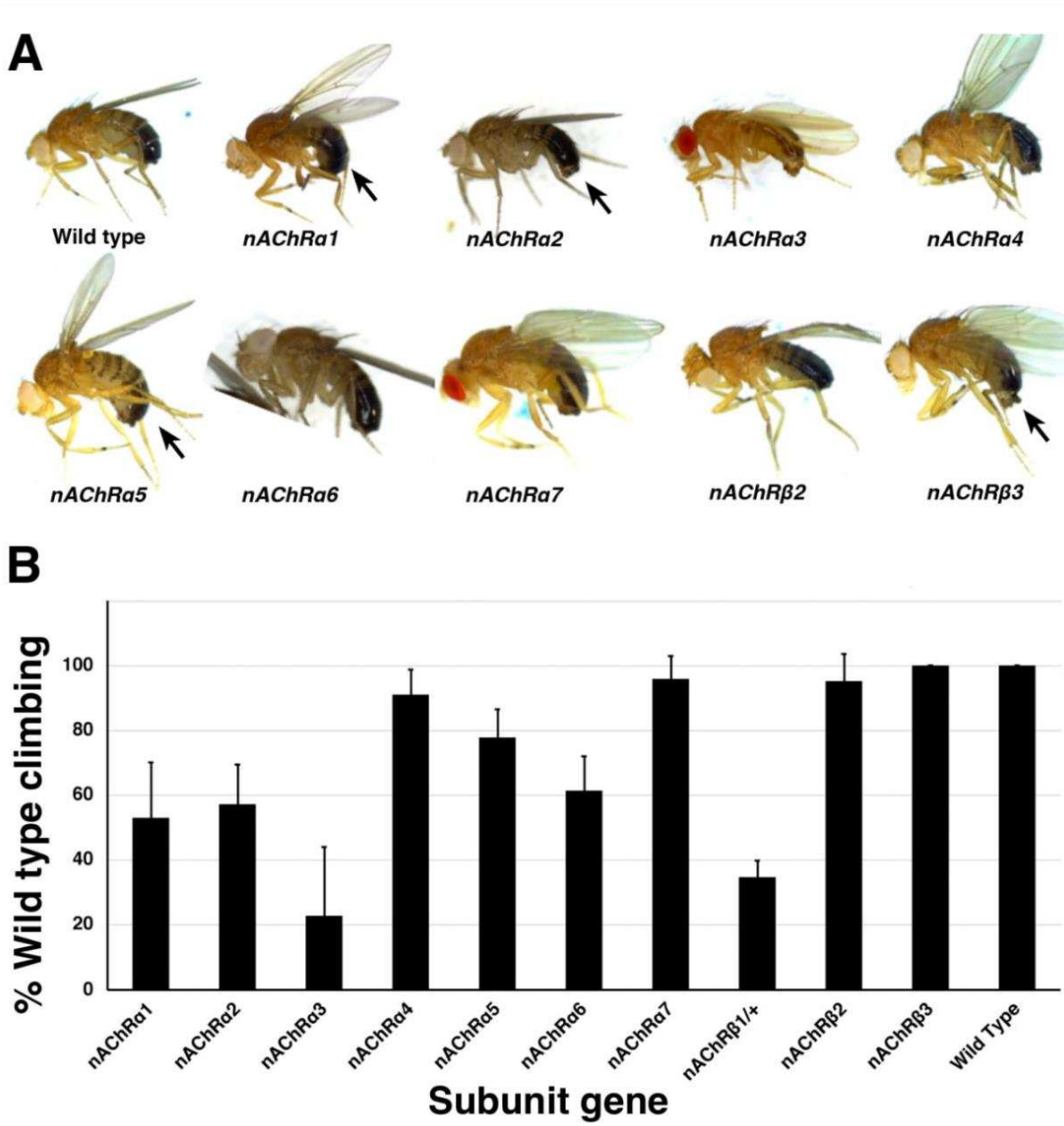
152 exhibited a severe reduction in locomotor activity to less than 40 % of wild-type (22% and 34%

153 respectively).

154 Taken together, we report the generation and validation of null mutations in all ten *D.*

155 *melanogaster* *nAChR* subunit genes, with mild morphological defects associated with most of

156 the new alleles and impaired locomotion observed with some mutants.



158 **Figure 1. Morphological and locomotor phenotypes in *nAChR* subunit mutants.**

159 (A) Adult males from indicated *nAChR* subunit null mutants. Arrows indicate strong curled abdomen

160 phenotypes. (B) Graph of locomotor activity determined in climbing assays as a percentage of wild

161 type. Error bars represent standard deviation from 5 replicates.

162 **Distinct nAChR subunits mediate interactions with ω -Hexatoxin-Hv1a and α -
163 Bungarotoxin**

164 In order to investigate the selective contribution of each *nAChR* subunits to toxin binding *in*
165 *vivo*, we injected 3rd instar larvae from the homozygous *nAChR* null mutants with either ω -
166 Hexatoxin-Hv1a (Hv1a) or α -Bungarotoxin (α -Btx) dissolved in PBS. As a control, injections
167 of PBS alone (vehicle) were performed in parallel, and all larvae survived the injection
168 procedure and showed no detectable defects. Larval injection of 2.5 nmol/g Hv1a induced
169 locomotor paralysis and full lethality in the control groups (*w*¹¹¹⁸, *THattP40* and *THattP2*,
170 Figure 2A, Appendix-table 2). Survival was quantified as the percentage of pupae formed after
171 injection. Hv1a did not result in full lethality with *nAChRa4* and *nAChR β 2* homozygous
172 mutants, since both showed an increase in survival to 42±22% (One-way ANOVA followed
173 by Bonferroni's test, $P=0.0035$, Figure 2A). Mortality in all the other null mutants was
174 comparable to controls ($P>0.9$).

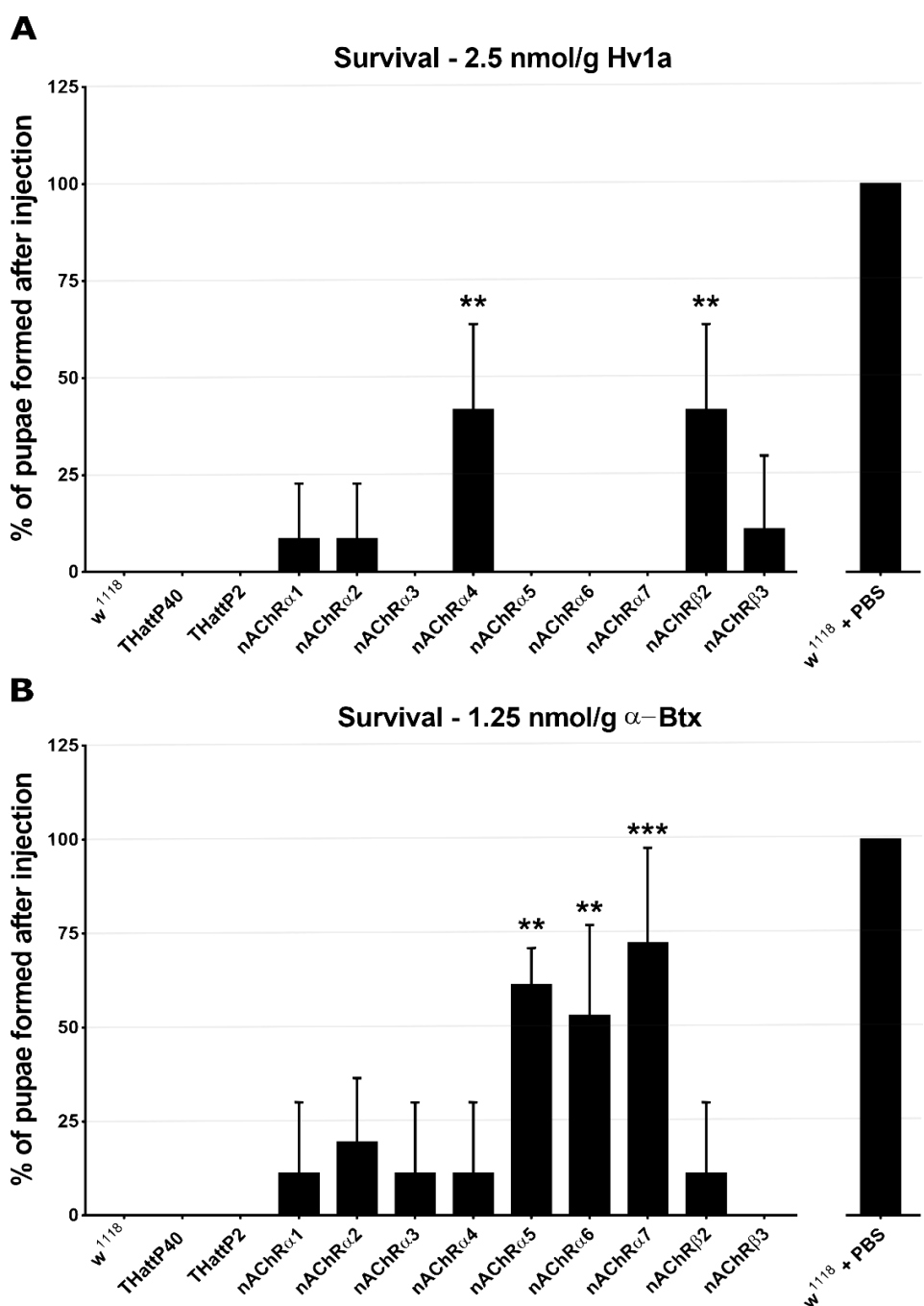
175 We also observed significant toxicity following injection of 1.25 nmol/g α -Btx, with larvae
176 exhibiting a progressive reduction in locomotion until stationary, resulting in developmental
177 arrest and death. We found that α -Btx induced lethality is drastically reduced in the *nAChRa5*,
178 *nAChRa6* and *nAChRa7* subunit mutants, with the survival rate significantly increased from
179 0% (controls) to 61±10% ($P=0.001$), 53±24% ($P=0.0051$) and 72±25% ($P=0.0001$)
180 respectively (One-way ANOVA followed by Bonferroni's test, Figure 2B).

181 Together, these results indicate that Hv1a and α -Btx do not share the same binding target and
182 differentially interact with the nAChR subunits *in vivo*. Since α -Btx showed a novel insecticidal
183 effect on nAChRs we further examined its interactions biochemically.

184

185

186



187

188 **Figure 2. ω -Hexatoxin-Hv1a and α -Bungarotoxin target different nAChR subunits.**

189 (A) Bar graph of the survival rate, measured as the percentage of pupae formed, following larval
190 injection of 2.5 nmol/g Hv1a in the indicated homozygous lines. Mean \pm SD of 3 independent replicates
191 of 10 larvae per replicate. ** $P=0.0035$ (one-way ANOVA ($F_{(11,24)}=4.99$, $P=0.0005$ with Bonferroni's
192 multiple comparisons test). 3 independent replicates in each group (10 injected larvae in total). (B)
193 Survival rate following larval injection of 1.25 nmol/g α -Btx. Mean \pm SD of 3 independent replicates
194 of 10 larvae per replicate. ** $P<0.001$, *** $P=0.0001$ (one-way ANOVA ($F_{(11,24)}= 7.921$, $P<0.0001$,
195 followed by Bonferroni's multiple comparisons test). 3 independent replicates in each group (10
196 injected larvae in total). w^{1118} is the wild type base stock, THattP40 and THattP2 are the Cas9 lines used
197 to establish the mutants, w^{1118} + PBS represents the injection control.

198

199 **Forming SMA-lipid particles (SMALPs) of ring-like nAChR complex structures**

200 In order to take advantage of our new receptor subunit mutants for the biochemical analysis of
201 native nAChR functions, we examined the composition of the receptors responsible for binding
202 α -Btx. To address the functionality of *D. melanogaster* nAChRs isolated from endogenous
203 membranes, we utilised detergent-free SMALPs extraction to characterise the interaction
204 between receptor native lipid discs and the α -Btx toxin (Figure 3A).

205

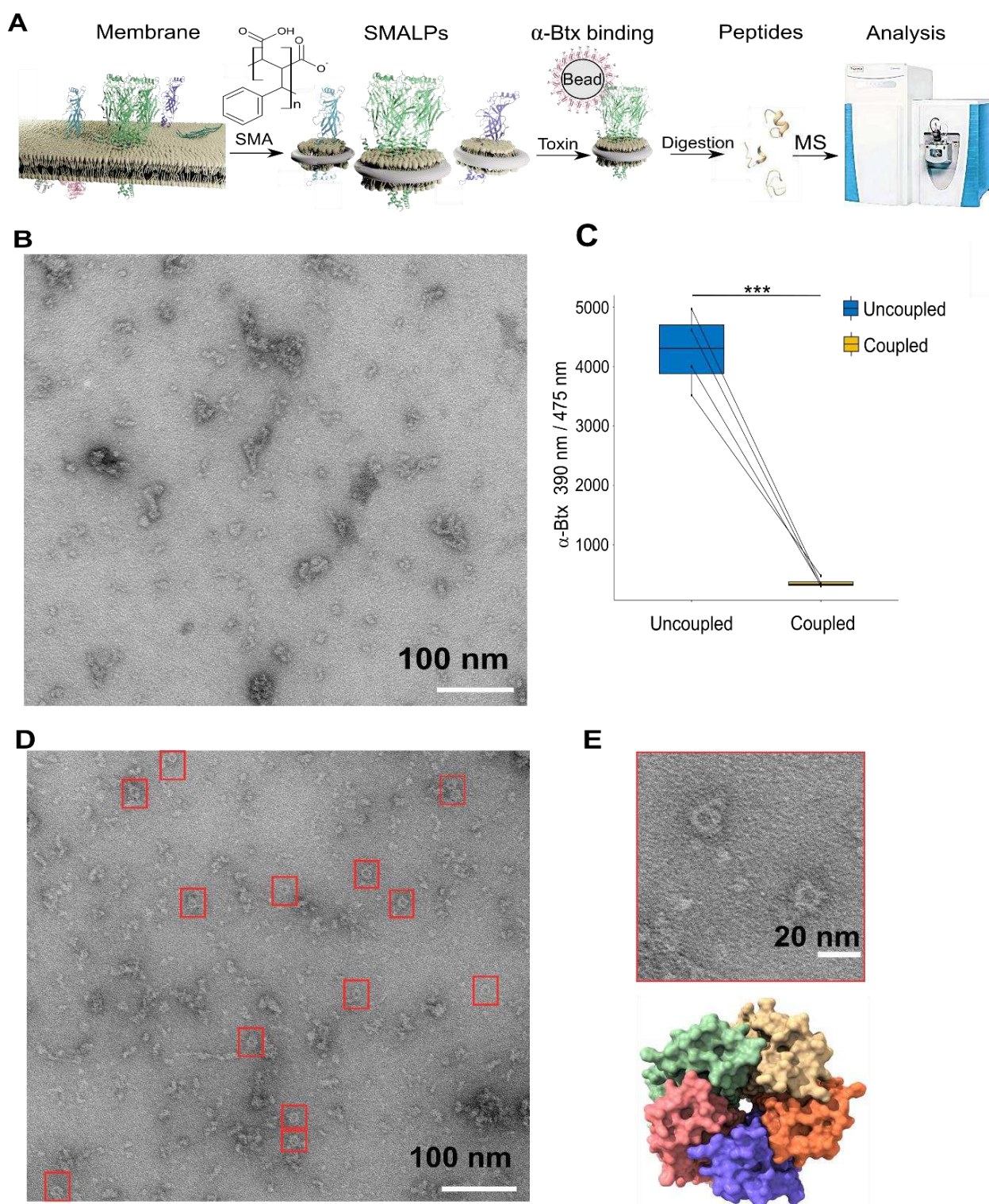
206 In brief, we prepared membrane extracts from adult *D. melanogaster* heads (Depner et al.,
207 2014) and generated lipid particle discs by solubilising the membrane extracts with the SMA
208 copolymer. We used affinity beads coupled to α -Btx (Wang et al., 2003; Mulcahy et al., 2018)
209 to enrich for nAChRs in the SMALP preparations that bound to the toxin, and performed mass
210 spectrometric analysis of tryptic peptides generated from the enriched preparations. In parallel
211 we processed membrane extracts without SMALP and with SMALP extracts enriched with
212 beads alone.

213 We first determined whether membrane protein discs are formed from enriched membranes
214 using the SMA copolymer. We prepared membrane enriched fractions from adult heads,
215 solubilized these with SMA and separated the insoluble particles from the lipid discs by
216 ultracentrifugation. We negatively stained the SMALP preparations and imaged them with
217 transmission electron microscopy (TEM), observing irregular discs of varying shapes and
218 sizes, with clusters containing different numbers of discs (Figure 3B).

219 Membrane receptors often have a unique shape in TEM images and the five subunits of a
220 nAChRs is expected to form a ring-like structure, suggesting that the receptors are extracted as
221 a complex. However, we did not observe pentameric ring-like structures perhaps suggesting
222 that nAChRs are of low abundance and that analysis may benefit from enrichment. We coupled
223 α -Btx to affinity beads to enrich nAChR complexes that bind the toxin in SMALP preparations
224 (Figure 3C). In contrast to the unenriched samples, TEM images of the enriched preparations
225 showed increased numbers of ring-like structures of 15 nm in diameter (Figure 3D, E). Thus
226 our TEM analysis shows an increased number of ring-like membrane complexes in the SMALP
227 preparations which are likely to be nAChRs.

228

229



230
231

Figure 3. Forming styrene maleic acid lipid particles (SMALPs).

232 (A) Schematic representation of the SMALPs extraction and nAChRs pull-down for mass spectrometric
233 analysis. (B) Negative staining of extracted SMALPs by transmission electron microscopy. Scale bar
234 100 nm. (C) Fluorescence signal of uncoupled α -Btx in solution before and after coupling to affinity
235 beads (two-tailed t-test, *** $P<0.001$, n=4). (D, E) Negative staining of extracted SMALPs after α -Btx
236 pull-downs. Ring-like protein structures are boxed (Scale bar = 100 nm) with an example in the
237 magnified image (Scale bar = 20 nm). A top view of the nAChR structure from PDB entry 4HQP is
238 shown for reference.

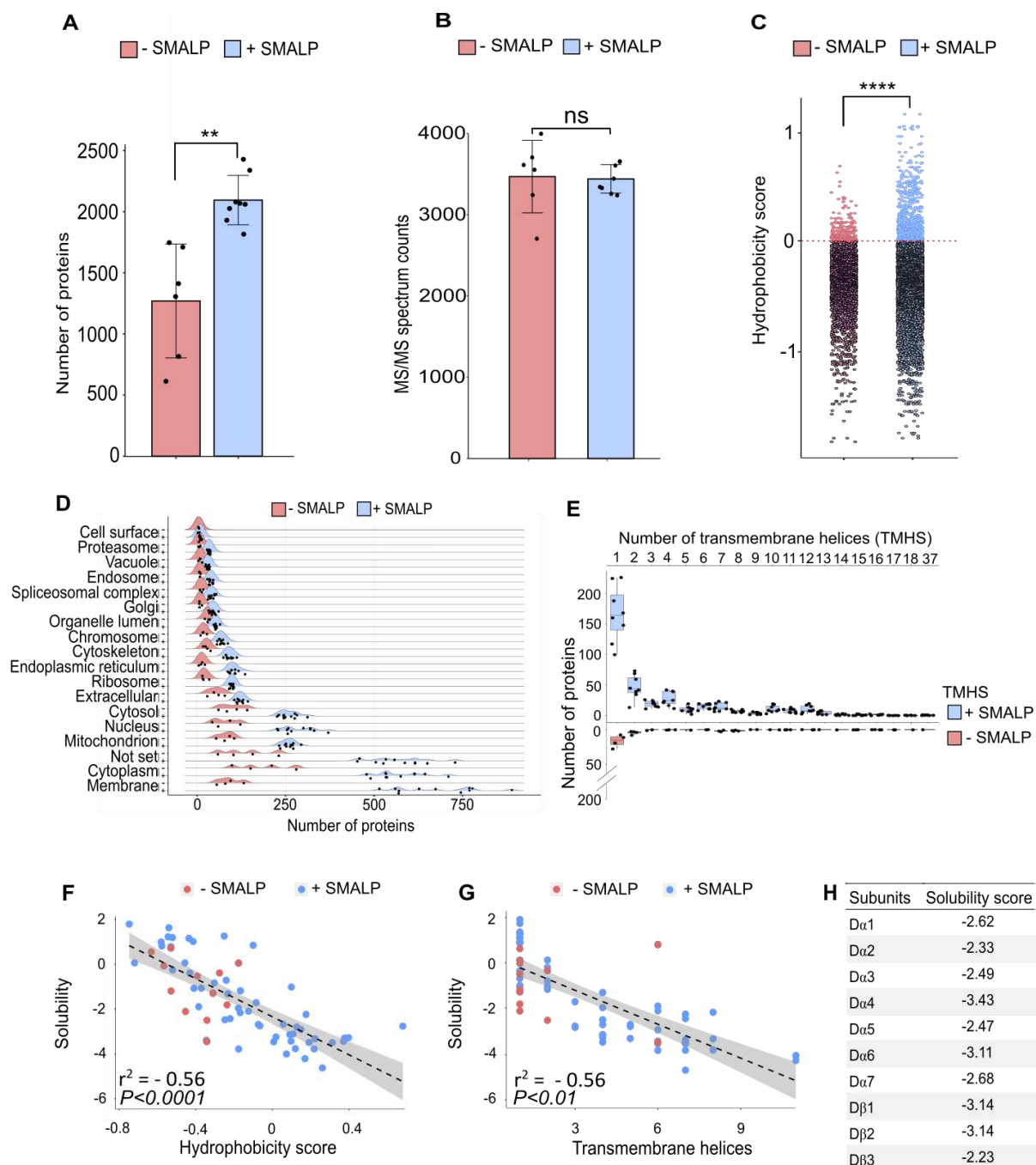
239 **Efficient SMALPs extraction allow to study nAChR subunits solubility**

240 To assess to what extent the SMA copolymer solubilized nAChRs, we performed a bottom-up
241 proteomics analysis to identify receptor subunits. Membrane preparations were solubilized in
242 buffer with or without SMA, and affinity beads with or without α -Btx were used to assess
243 ligand-binding to nAChR subunits. Comparing the number of proteins identified in samples
244 solubilized either with or without 5% SMA, we observed a significantly increased
245 identification rate of proteins dissolved in SMA by equal numbers of MS/MS spectral counts
246 (two-tailed t-test, $P<0.01$, Figure 4A and non-significant, Figure 4B). This indicates that mass
247 spectrometer performance was comparable during the measurements.

248 Sequences of membrane spanning segments of nAChR subunits, which are in close contact to
249 the hydrophobic lipid environment, are largely composed of nonpolar side chains. Determining
250 the average of hydrophobicity of identified protein sequences revealed significantly increased
251 numbers of proteins with a positive hydrophobicity score in samples solubilized in SMA (two-
252 tailed t-test, $P<0.0001$, Figure 4C), indicative of enrichment of membrane proteins. An analysis
253 of Gene Ontology (GO) slim terms supports the conclusion that the SMALP preparations are
254 enriched of membrane embedded and associated proteins (Figure 4D), and that these are not
255 limited to plasma membrane proteins. In the SMA-enriched samples we found enrichment for
256 proteins annotated with metabolic and catalytic activity terms and also enhanced response to
257 biological stimuli (Figure 4-figure supplement 1A, B), highlighting the recovery of membrane-
258 associated proteins.

259 Next, we focused on identified membrane proteins predicted to contain transmembrane helical
260 (TMH) domains and found an increased number of proteins containing TMHs in SMA
261 solubilized samples (Figure 4E). While the majority of these proteins contained a single TMH
262 domain, we identified Piezo, a mechanosensory ion channel protein containing 37 predicted
263 transmembrane helices. Both α - and β -nAChR subunits contain four TMH domains and could
264 be solubilized in SMA. The number of β -barrel membrane spanning proteins identified was
265 also significantly increased by SMA extraction (two-tailed t-test, $P<0.0001$, Figure 4-figure
266 supplement 1C). In addition, palmitoylated lipid anchor modifications to nAChR subunits has
267 been shown to be important for receptor assembly into membranes and the formation of
268 functional complexes (Alexander et al., 2010).

269



270

271 **Figure 4. Identification of proteins enriched by SMALP extraction.** (A) Number of identified
 272 proteins in affinity pull-down samples solubilized with or without SMA, two-tailed t-test, $**P < 0.01$,
 273 $n=6$ or 8 replicates per condition. (B) MS/MS spectrum counts from samples solubilized with or without
 274 SMA, ns = not significant after two-tailed t-test with $n=6$ or 8. (C) Calculated hydrophobicity score of
 275 amino acid residues found in protein sequences obtained with and without SMA solubilisation,
 276 $****P < 0.0001$, two-tailed t-test, $n=3$ per condition. (D) GO term (cellular compartment) enrichment of
 277 proteins identified with and without SMA solubilisation, $n=4$ or 11. (E) Predicted numbers of proteins
 278 containing transmembrane helices obtained with or without SMA solubilisation, $n=4$ or 8. (F, G)
 279 Analysis of solubility and hydrophobicity of receptors identified with and without SMA solubilisation
 280 ($r^2 = -0.56$, $P < 0.0001$, $n=4$) and of transmembrane receptor helices ($r^2 = 0.56$, $P < 0.01$, $n=4$). (H)
 281 Solubility score of individual nAChR subunits.

282 Comparing samples solubilized with and without SMA showed a significantly increased
283 identification of proteins which are predicted to be palmitoylated and myristoylated (two-tailed
284 t-test, $P<0.0001$, Figure 4-figure supplement 1D, E). In contrast, membrane proteins that are
285 predicted to contain a glycosylphosphatidylinositol (GPI)-anchor are equally solubilized in
286 both conditions (two-tailed t-test, non-significant, Figure 4-figure supplement 1F).

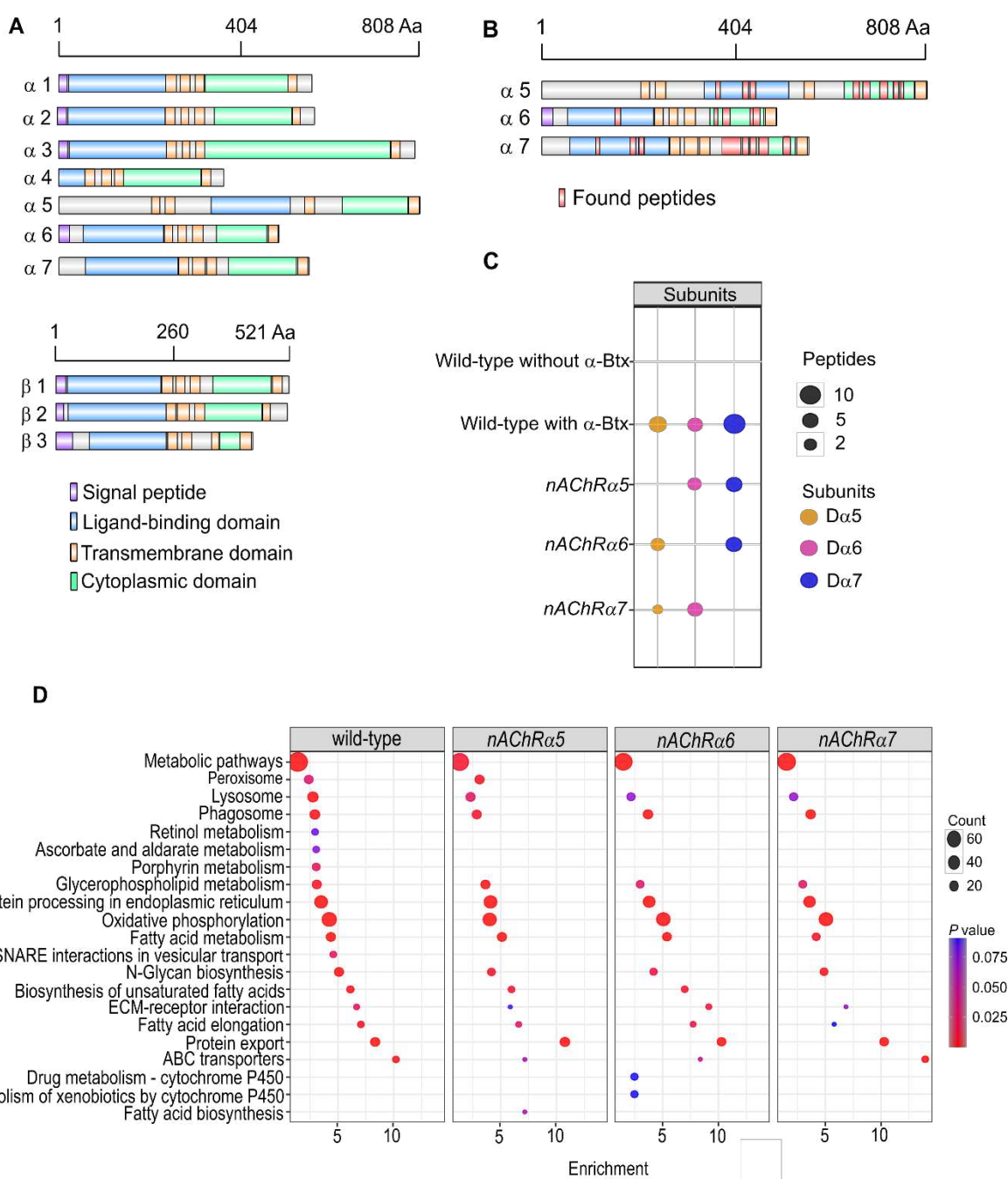
287 Focusing on the membrane receptors solubilized by SMA, we analysed the amino acid
288 sequence properties of identified proteins and calculated an overall solubility score (Sormanni
289 et al., 2015; Sormanni et al., 2017). Comparing the solubility to the hydrophobicity showed a
290 calculated R^2 of 0.56 (Figure 4F). Sequences with a score greater than 1 are highly soluble
291 receptors and those less than minus -1 are difficult to solubilize. As a result, samples solubilized
292 in SMA contain more receptors, which are difficult to solubilize. These receptors are more
293 hydrophobic and contain larger numbers of TMH domains (Figure 4G). Calculating an average
294 solubility score of -2.76 for nAChR sequences indicates that difficult to solubilize subunits are
295 successfully recovered with SMA (Figure 4H).

296 Taken together, these analyses confirm that SMA solubilizes nAChR complexes in a state
297 suitable for subunit identification by mass spectrometry and suggests that α -Btx interactions
298 can be studied with SMALP preparations.

299 **Three nAChR α -subunits are targets of α -Btx**

300 To explore native nAChR subunit interactions with α -Btx we searched for peptides from
301 subunit ligand-binding and cytoplasmic domains, identifying the D α 5, D α 6 and D α 7 subunits
302 in the α -Btx affinity bead pull-downs (Figure 5A and B, Appendix-table 3). Several other
303 nAChR subunit peptides could be identified in the negative controls performed without
304 coupling α -Btx to affinity beads (Appendix-table 4). The sequences of the ligand-binding
305 domains of the D α 5, D α 6 and D α 7 subunits are very similar (avg. 95.49 %) and we identified
306 peptides common to all three subunits (Figure 5-figure supplement 2A) as well as unique
307 peptides within their cytoplasmic domains (Figure 5-figure supplement 2B). However, we
308 found no evidence of peptides mapping to TMH domains. The ligand-binding domain of α -
309 subunits show structural similarity across different species (Figure 5-figure supplement 3A)
310 and by mapping the identified peptides to known structures we concluded they are most likely
311 outside of the α -Btx binding sites (Figure 5-figure supplement 3B).

312



313

314 **Figure 5. Three nAChR α -subunits are binding to α -Bungarotoxin (α -Btx).**

315 (A) Graphical representation of ten nAChR subunits. The position of protein domains and signal
 316 peptides are shown. (B) Identified peptides of D α 5, D α 6 and D α 7 nAChR subunits in pull-downs using
 317 α -Btx affinity beads. Found peptides in ligand-binding and cytoplasmic domain are highlighted in red.
 318 (C) Numbers of identified unique peptides in wild-type pull-downs using affinity beads in absence and
 319 presence of α -Btx, n=3. Deleting nAChR α 5, nAChR α 6, nAChR α 7 and performing pull-downs identified
 320 unique peptides of nAChR subunits suggesting that functional complexes can be formed in null alleles,
 321 n=3. (D) KEGG pathway enrichment analysis of pull-downs in wild-type and nAChR α 5, nAChR α 6,
 322 nAChR α 7 null alleles, Fisher's exact test, n=3. Protein counts with P values of enriched pathways are
 323 shown. P values of ≤ 0.05 are to be considered as strongly enriched with default threshold of 0.1.

324

325 To further characterize the role of the three α -subunits identified in α -Btx binding we generated
326 SMALP preparations and performed α -Btx affinity bead enrichments with adult head
327 preparations from homozygous null mutations for each of the *nAChRa5*, *nAChRa6* and
328 *nAChRa7* subunit genes. With all three deletion mutants we observed, as expected, no
329 detectable peptides from the missing subunit but could still identify peptides from the other
330 two subunits (Figure 5C).

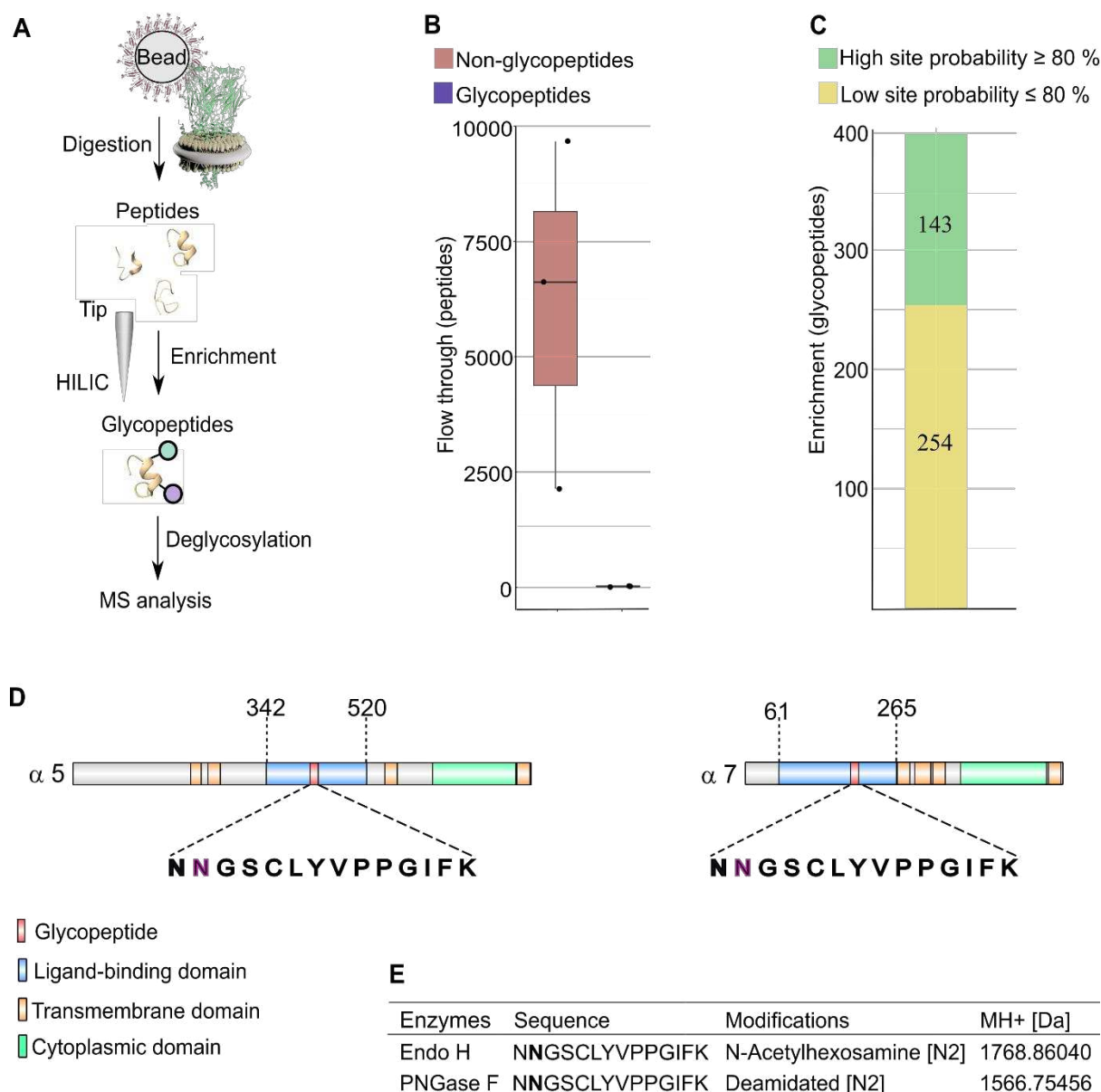
331 We compared the repertoire of proteins identified with α -Btx enrichment in wild-type with
332 those found in each of the three mutant lines to identify any changes in the representation of
333 biological pathways annotated in KEGG (Kanehisa et al., 2020, Figure 5D). While the
334 enrichments in wild-type and the mutants were broadly similar, we noticed a loss of proteins
335 associated with cofactor/vitamin metabolism, particularly retinol and ascorbate, in all three of
336 the mutants as well as proteins associated with vesicular transport. It is possible that these
337 pathway changes represent alterations in neurotransmitter production or trafficking.
338 Interestingly, we also noticed specific enrichment of cytochrome P450 related pathways in the
339 *nAChRa6* mutants, suggesting perturbation of neurotransmitter pathways.

340 In summary, our analysis indicates that a functional α -Btx binding nAChR involves the $\text{D}\alpha 5$,
341 $\text{D}\alpha 6$ and $\text{D}\alpha 7$ subunits. This is entirely in line with our genetic findings described above, where
342 loss of each of these subunit genes conferred substantial resistance to α -Btx induced lethality.

343 **Glycosylation sites of nAChR subunits by α -Btx binding**

344 We next examined glycosylation sites on nAChR subunits since these are known to have an
345 important role in α -Btx binding affinity in other systems. For example, deglycosylation reduces
346 α -Btx binding in human nAChRs by more than two orders of magnitude (Dellisanti et al., 2007)
347 and α -Btx binding to loop C in *Torpedo californica* α -subunits is enhanced by N-glycosylation
348 of sites in these regions (Rahman et al., 2020). To identify specific glycosylation sites in *D.*
349 *melanogaster* nAChRs we first purified SMALP solubilized receptors with α -Btx affinity
350 beads, digested them into peptides and enriched for glycopeptides using HILIC resin
351 (Hägglund et al., 2004, Figure 6A). Site-specific identification of glycans on peptides by mass
352 spectrometry is challenging (Fang et al., 2020) and often requires an additional deglycosylation
353 step for glycopeptide measurement.

354



355

356 **Figure 6. N-glycosylation sites in nAChR subunits.**

357 (A) Diagrammatic representation of nAChR subunit glycopeptide enrichment. Pull-downs with α-Btx
 358 affinity beads enrich for nAChRs and after tryptic digestion glycopeptides were enriched.
 359 Glycopeptides were deglycosylated with Endo H or PNGase F and analyzed by mass spectrometry. (B)
 360 Low numbers of glycopeptides (average 20) are detected in flow through fractions. (C) Numbers of
 361 identified glycopeptides according to site probabilities are shown (n=3). (D) Shared glycopeptide
 362 identified in the ligand-binding domain of $\alpha 5$ and $\alpha 7$, an N-linked glycosylated asparagine (N)
 363 residue is highlighted. (E) Deglycosylated peptide with either Endo H or PNGase F and contains either
 364 an N-acetylhexosamine or is deamidated on asparagine (N2). The two different modifications on the
 365 same peptide lead to a different monoisotopic mass (MH+ [Da]). Peptide contains an additional
 366 carbamidomethyl on cysteine (C5).

367

368

369 Deglycosylation of enriched peptides was carried out using two separate enzymes:
370 Endoglycosidase H (Endo H), which cleaves asparagine-linked oligosaccharides to generate a
371 truncated sugar molecule with one N-acetylhexosamine (HexNAc) residue, and the
372 endoglycosidase PNGase F, which releases the entire glycan from asparagine residues and
373 deaminates the sugar free asparagine to aspartic acid. While very few glycopeptides were
374 observed in the flow through (an average 20 glycopeptides Figure 6B), we identified a total of
375 397 glycopeptides after enrichment and deglycosylation with Endo H or PNGase F (Figure
376 6C).

377 Shared glycopeptides from D α 5 and D α 7 nAChR subunits were identified after enrichment
378 and deglycosylation with Endo H or PNGase F (Figure 6D). Deglycosylation with Endo H
379 identified modified asparagine (N2) residues on the peptide (NNGSCLYVPPGIFK), which is
380 predicted to be part of the D α 5 and D α 7 ligand-binding domains involved in α -Btx binding.
381 This asparagine residue was modified with an N-acetylhexosamine (HexNAc) truncated sugar
382 chain. Releasing N-glycans after deglycosylation by PNGase F enabled us to identify a
383 deaminated asparagine residue in the same peptide. The monoisotopic mass of this peptide
384 changed due to the different modifications on the asparagine residue (Figure 6E).

385 The genome of *Caenorhabditis elegans* encodes for at least 29 nAChR subunits (Jones et al.,
386 2007). The alpha-type unc-63 subunit contains an N-linked HexNAc modified asparagine
387 residue on position 136 (Kaji et al., 2007). Performing a multiple sequence alignment showed
388 that this asparagine residue is conserved between insects and nematodes (Figure 6-figure
389 supplement 4A). Comparing identified glycosylation sites of D α 5 and D α 7 subunits to known
390 N-linked glycosylation sites of α -subunits from *T. californica*, *Danio rerio*, *Mus musculus* or
391 *Homo sapiens* indicates that this site is not conserved between vertebrates and invertebrates
392 (Figure 6-figure supplement 4B).

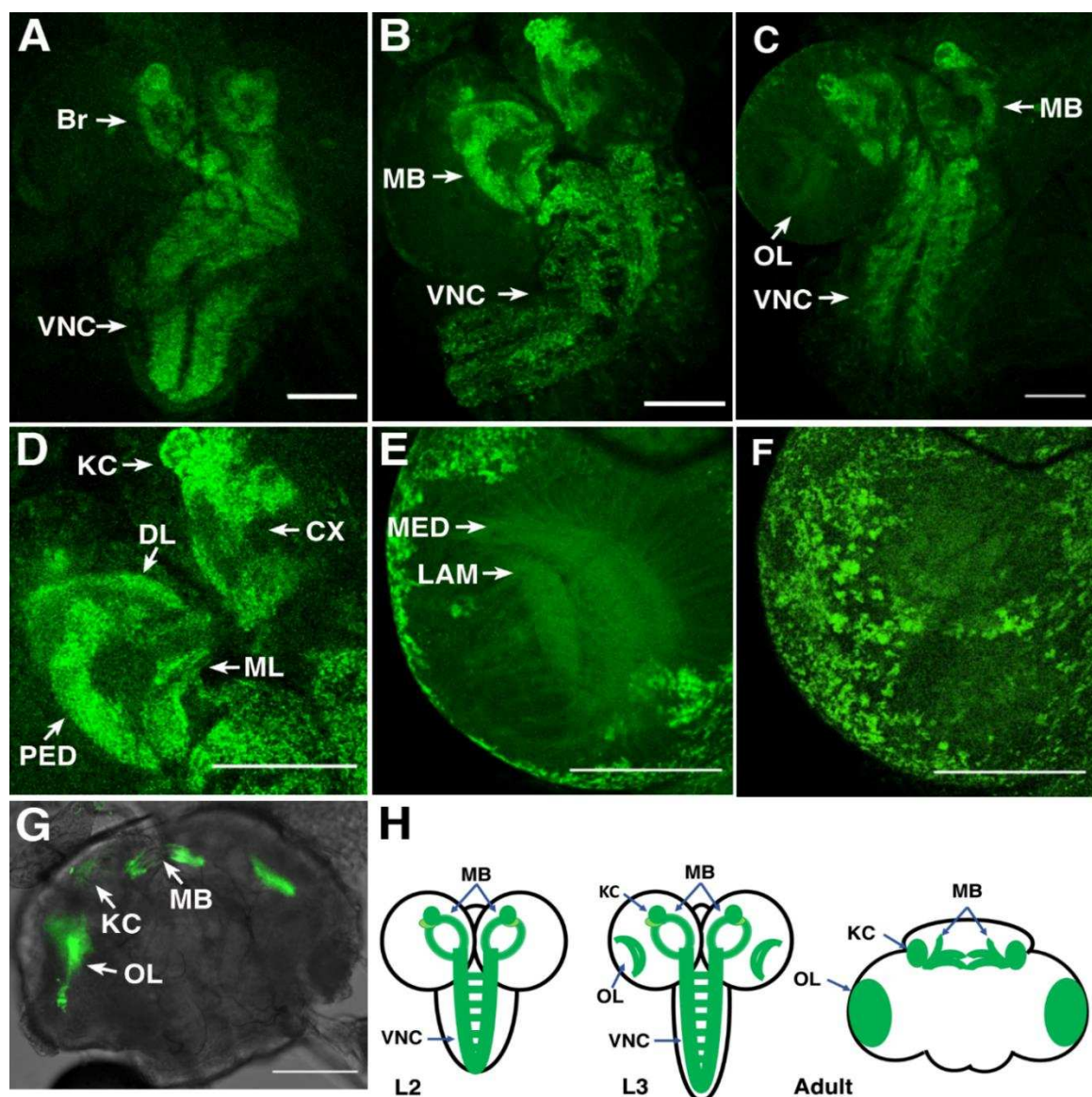
393 We also identified glycosylation sites in the D α 3 (ATKATLNYTGR) and D β 3
394 (VVLPGNTAR) subunits after Endo H treatment but not with PNGase F treatment,
395 suggesting they harbour a single N-linked HexNAc modified asparagine residue (Figure 6-
396 figure supplement 4C).

397 Taken together these findings suggest that the D α 5 and D α 7 subunits are modified at
398 asparagine residues in the α -Btx ligand-binding domain with an N-linked sugar chain.

399

400 **Localization of D α 6 nAChRs subunit in the brain**

401 In order to examine the endogenous localization of an α -Btx binding receptor subunit we used
402 CRISPR/Cas9 genome engineering to introduce in frame C-terminal fluorescence and epitope
403 tags into the endogenous *nAChR α 6* locus (Figure 7).



404
405 **Figure 7. *In vivo* imaging of endogenously tagged D α 6 nAChR subunit.** (A-G) Live imaging
406 of fly brains carrying a C-terminal EGFP fusion into the endogenous *nAChR α 6* locus. (A-C) D α 6
407 subunit in 2nd, early and late 3rd instar larvae brain, respectively. Visible localization in ventral nerve
408 cord (VNC), mushroom bodies (MB), and optic lobes (OL). Scale bar = 100 μ m. (D) D α 6 subunit in
409 mushroom bodies of 3rd instar larvae with detectable fluorescence signal in Kenyon cells (KC), calyx
410 (CX), peduncle (PED), dorsal lobes (DL) and medial lobes (ML). Scale bar = 100 μ m. (E) D α 6 subunit
411 was observed in developing optic lobes, lamina (LAM) and medulla (MED) of later 3rd instar larvae.
412 Scale bar = 100 μ m. (F) D α 6 subunit on the external structures of developing lobes in later 3rd instar
413 larvae. Scale bar = 100 μ m. (G) D α 6 subunit in adult fly brain, strong signal detected in mushroom
414 bodies (MB) and optic lobe (OL). Scale bar = 100 μ m. (H) Schematic summary of D α 6 subunit
415 expression during different developmental stages, 2nd and 3rd instar larvae and adult fly, (L2, L3 and
416 Adult, respectively) in which the green lines indicate the localization of the D α 6 subunit.

417 The resulting line is homozygous viable and fertile, and shows no apparent phenotypes. We
418 live imaged the unfixed brains of larvae and adults homozygous for the tagged line using
419 confocal microscopy. In 2nd instar larvae we observed low level well-distributed fluorescence
420 signal throughout the ventral nerve cord (VNC), including on commissural axons, and in the
421 developing brain (Figure 7A).

422 By early L3, we found more defined localization in the VNC and developing mushroom bodies
423 (Figure 7B and D), particularly noticeable in the Kenyon cells, a known site of α -Btx binding
424 (Su & O'Dowd, 2003). Localization in larval mushroom bodies continued to evolve, with
425 defined expression in the Kenyon cells, calyx, peduncle, dorsal and medial lobes as well as the
426 medulla and lamina of the emerging optic lobes (Figure 7C, E). We also observed localisation
427 to a number of cell bodies overlying the optic lobes (Figure 7F).

428 Finally, in the adult brain, expression was largely restricted to the mushroom bodies
429 particularly the Kenyon cells and connections across the midline between the β and γ lobes and
430 the optic lobes (Figure 7G). The temporal localization of Da6 subunit in the CNS is
431 summarized in schematic form (Figure 7H).

432 Discussion

433 Elucidation of complex insect nAChRs heterogeneity will lead to a better understanding of
434 selective insecticidal effects. We present a new set of null mutations in all *D. melanogaster*
435 nAChR subunit genes and investigated insecticidal peptide toxin effects on wild-type and
436 receptor subunit mutant larvae. Utilising biochemical approaches with SMALP pull-downs we
437 characterised toxin binding and subunit composition of native nAChR complexes.

438 Our genome engineering approach generated viable and fertile mutations in nine out of the ten
439 subunit genes encoded in the *D. melanogaster* genome and is largely concordant with the
440 recently described work by Perry and colleagues (Perry et al., 2021). In both studies, null
441 mutations in the *nAChR β 1* gene were inviable as stocks. We add to the previous work by
442 generating viable mutations in *nAChR α 5*. We observed some minor morphological defects in
443 some of the null mutants especially in *nAChR α 1*, *nAChR α 2*, *nAChR α 5* and *nAChR β 3* as well
444 as locomotor defects with some alleles, particularly severely in *nAChR α 3* homozygotes and
445 *nAChR β 1* heterozygotes. The locomotor defects we observed are in agreement with previously
446 reported neuronal phenotypes with nAChR subunit genes, including sleep disruption, defective
447 jump response, memory impairment or locomotor defects (Fayyazuddin et al., 2006; Rohde et
448 al., 2016; Somers et al., 2017; Tackenberg et al., 2020).

449 We used the nAChR null mutants to study insecticidal effects of the Hv1a peptide on viability
450 after injection into larvae and investigated whether α -Btx has any insecticidal properties. As
451 described by Chambers and colleagues, we confirm that Hv1a effects nAChRs (Chambers et
452 al., 2019) and our analysis shows that the D α 4 and D β 2 subunits are involved in the insecticidal
453 response. We show for the first time that α -Btx has selective insecticidal effects against the
454 D α 5, D α 6 and D α 7 subunits, which we further characterized at the biochemical level.

455 The pharmacology of Hv1a and α -Btx binding has been shown to be distinctive (Chambers et
456 al., 2019), correlating with our demonstration that these two peptide toxins mediate their effects
457 through different receptor alpha subunits. Furthermore, resistance to neonicotinoid
458 insecticides, which interact most strongly with Hv1a binding, has been associated with D β 2
459 (Perry et al., 2008; Perry et al., 2021), consistent with the involvement of this subunit in the
460 response to Hv1a. However, no resistance to neonicotinoids was seen in *D. melanogaster*
461 carrying a *nAChRa4* gene deletion (Perry et al., 2021), which could be explained if
462 neonicotinoids act at multiple receptor classes. Multiple binding sites for the neonicotinoid
463 imidacloprid can be resolved in equilibrium binding assays in many insect species (Xu et al.,
464 2010) and by binding kinetics in flies (Liu & Casida, 1993).

465 Resistance to spinosad is strongly associated with D α 6 (Perry et al., 2021), and spinosad
466 binding is much more sensitive to the action of α -Btx than to the action of neonicotinoids
467 (Chambers et al., 2019), again consistent with the involvement of this subunit with sensitivity
468 to injected α -Btx and with the proposition that α -Btx and Hv1a act at distinct receptor classes.

469 nAChR subunits are known to be difficult to purify due to solubilisation issues (Cheng et al.,
470 2015; Maldonado-Hernández et al., 2020) and the requirement for a lipid environment for
471 ligand binding (Dacosta et al., 2013) makes it challenging to study these receptors in native
472 conditions. We used the SMALPs extraction method for preparing membrane discs and
473 enriched nAChRs via α -Btx affinity purification. Electron microscopy analysis indicated that
474 receptor-like particles were recovered and these were substantially enriched by α -Btx pull-
475 down. Mass spectrometry analysis showed an enrichment for the D α 5, D α 6 and D α 7 subunits
476 in these preparations, which is concordant with our *in vivo* injection results and previous studies
477 that characterised aspects of α -Btx binding (Lansdell & Millar, 2004; Wu et al., 2005; Lansdell
478 et al., 2012).

479 To our knowledge this is the first report of the identification of a native endogenous α -Btx
480 binding nAChRs. We note however, that we cannot determine from our analysis whether all

481 three identified subunits are part of the same complex or if there are different receptors
482 containing a subset of these subunits. Using chimeric receptors in a cell line system, Lansdell
483 and colleagues reported that a combination of all three of these subunits show high affinity
484 acetylcholine binding but α -Btx binding varied depending on receptor combinations, with $\text{D}\alpha 5$
485 and $\text{D}\alpha 6$ binding most strongly (Lansdell et al., 2012). In a prior study they implicated $\text{D}\alpha 6$
486 and $\text{D}\alpha 7$ (Lansdell & Millar, 2004). However, these assays were performed with 5HT3A-
487 nAChR subunit fusions, here we provide strong evidence that these three subunits bind to α -
488 Btx *in vitro* and *in vivo*.

489 In addition, glycopeptide enrichment showed site specific glycosylation modifications on the
490 $\text{D}\alpha 5$ and $\text{D}\alpha 7$ nAChR subunit ligand binding domains. The unique lipid environment and
491 glycosylation sites of nAChR α -subunits from the electric ray, *T. californica*, were found to be
492 important for α -Btx binding activities (Quesada et al., 2016; Rahman et al., 2020), and
493 structural studies support this conclusion (Dellisanti et al., 2007). Our work supports the view
494 that there is a role for $\text{D}\alpha 5$ and $\text{D}\alpha 7$ glycosylation modifications in the recognition of α -Btx in
495 *D. melanogaster*.

496 Our localization studies with fluorescence tagged endogenous $\text{D}\alpha 6$ subunit showed relatively
497 restricted expression in the brain and ventral nerve cord, with prominent expression in the
498 Kenyon cells of the mushroom body, all known regions. The expression of $\text{D}\alpha 6$ in Kenyon
499 cells across development is in line with a proposed role for this subunit in memory plasticity,
500 along with other α -subunits including $\text{D}\alpha 5$, in mushroom body output neurons (Barnstedt et
501 al., 2016). Thus, it is possible that retention of α -Btx binding in the absence of $\text{D}\alpha 6$ may simply
502 reflect its restricted localisation. In contrast, it is clear that $\text{D}\alpha 6$ plays a major and specific role
503 in binding to the insecticide spinosad in *D. melanogaster* since mutations in this subunit are
504 highly resistant to the toxin (Perry et al., 2015).

505 Localization studies of $\text{D}\alpha 6$ nAChRs subunit fusion protein by confocal microscopy are largely
506 consistent with recent reports of *nAChRa6* expression derived from expression reporters
507 (Kondo et al., 2020), though these studies appear to indicate wider adult brain expression than
508 we observed, perhaps reflecting a degree of translational control or limitations in the sensitivity
509 of our live imaging. In conclusion, we identified ligand-binding subunit sites for a *D.*
510 *melanogaster* nAChR antagonist with newly insecticidal effects. Our findings contribute to a
511 better understanding of the role of nAChR subunits which interacts with insecticidal peptide
512 toxins.

513 **Materials and methods**

514 **Drosophila methods**

515 Embryos were injected using standard procedures into the *THattP40* (y^l *sc* v^l *sev*²¹; $P\{y^{+l7.7}$
516 $v^{+l1.8}$ *nos-Cas9.R* $\}attP40$) or *THattP2* (y^l *sc* v^l *sev*²¹; $P\{y^{+l7.7}$ $v^{+l1.8}$ *nos-Cas9.R* $\}attP2$) lines
517 expressing *nos*-Cas9 (Bloomington *Drosophila* Stock Centre). Donor DNA (500 ng/ μ L) in
518 sterile H₂O was injected together with of gRNA plasmids (100 ng/ μ L) as described previously
519 (Korona et al., 2020). Individually selected surviving adults were crossed to w^{1118} and the
520 progeny screened for DsRED fluorescence localized mostly to the eyes of transgenic flies:
521 positive flies were balanced and homozygous stocks established where possible. The correct
522 localization of the insert was confirmed via PCR and sequencing. Transgenic flies were
523 assessed for the phenotype using bright field microscope. For tagging of *nAChRa6*, the stocks
524 were additionally subjected to Cre-recombination for marker removal and several independent
525 lines were verified by PCR. Some of these lines were screened for YFP fluorescence using
526 confocal microscopy. From the YFP positive balanced stocks, the viable and fertile
527 homozygote was established. Injections were performed by the Department of Genetics Fly
528 Facility (<https://www.flyfacility.gen.cam.ac.uk>). All fly stocks were maintained at 25°C on
529 standard cornmeal medium. Larvae of 2nd and 3rd stage were collected, and their brains were
530 dissected according to standard protocols. Brains were mounted in glycerol and live imaged.

531 **Cloning of gRNAs and generation of donor vectors**

532 **Construction of *nAChR* subunits null alleles**

533 In order to generate individual *nAChR* subunits gene deletions the open reading frame (ORF)
534 was disrupted by introducing a visible marker harbouring DsRED marker under eye specific
535 driver 3Px3 using CRISPR/Cas9 technology as previously described (Korona et al., 2020). The
536 targeted exons are shared between different isoforms and adjacent to the N-terminus to ensure
537 the protein translated was interrupted. The insertion sites were designed *in silico* and optimal
538 gRNAs were chosen (Appendix-table 5) that were tested against the injection strain and cloned
539 into pCDF3. Briefly, target specific sequences were synthesized and either 5'-phosphorylated
540 annealed and ligated into the *Bbs*I sites of pCDF3 precut with *Bbs*I. Positive clones were
541 confirmed by sequencing.

542 For generation of donor vectors, firstly, homology arms were amplified on genomic DNA
543 (Appendix-table 6) that, secondly, were used as a template to amplify the homology arms (

544 Appendix-table 7) of the donor vector for CRISPR/Cas9 homologous recombination (HDR).
545 The inserts with visible marker were amplified using as a template previously generated
546 constructs (Korona et al., 2020) with appropriate primers. These fragments were used for
547 Gibson assembly using Gibson Assembly Master Mix (New England Biolabs). PCR products
548 were produced with the Q5 High-Fidelity 2X Master Mix (New England Biolabs). All inserts
549 were verified by sequencing.

550 **C-terminal tagging of D α 6 nAChRs subunit fusion protein**

551 For tagging of D α 6 nAChRs subunit the C-terminal fusion with FSVS fluorescent protein
552 harbouring StrepII and 3xFLAG epitope tags (3xFLAG-StrepII-Venus-StrepII) was generated
553 for CRISPR/Cas9 mediated genome engineering (Korona et al., 2017; Korona et al., 2020).
554 Firstly, gRNAs were designed (Appendix-table 5) and tested against the genomic DNA
555 sequence of injection strains. The oligonucleotides were phosphorylated and ligated into *Bbs*I
556 pre-cut pCDF3. The positive variants were confirmed by sequencing.

557 The donor vector to generate protein fusion with fluorescent protein harbouring epitope tags
558 was cloned in 2 steps strategy by creating initially (A) nAChR α 6-FSVS donor and then adding
559 the removable marker to generate (B) nAChR α 6-FSVS-loxP-3PX3_DsRED_loxP donor
560 vector. At first, the homology arms were enriched on genomic DNA (Appendix-table 6) and
561 used to amplify homology arms for donor vector nAChR α 6-FSVS (Appendix-table 7) that was
562 assembled using Gibson Assembly® as described above. The FSVS tag was amplified on
563 previously generated constructs (Korona et al., 2017) with appropriate overlapping
564 oligonucleotides (Appendix-table 7). The construct was confirmed by Sanger sequencing and
565 used as a template to generate donor vector with removable marker. The PCR fragments
566 harbouring homology arms and FSVS tag were amplified on nAChR α 6-FSVS construct,
567 whereas the 3PX3-DsRed with adjacent loxP sites was amplified using earlier generated
568 constructs (Korona et al., 2017). The final donor vector was generated using Gibson
569 Assembly® as described above and positive variants were confirmed by sequencing.

570 **Confocal microscopy**

571 Localization of FSVS-tagged (3xFLAG-StrepII-Venus-StrepII) D α 6 nAChRs subunit was
572 visualised in dissected larvae brains via monitoring the YFP fluorescence (Venus). Briefly, the
573 larval brains were dissected and mounted in glycerol for live imaging. Images were acquired

574 using a Leica SP8 confocal microscope (Leica microsystems) with appropriate spectral
575 windows for mVenus, images were processed with Fiji software.

576 **Locomotor behaviour**

577 Adult female and male flies were collected shortly after eclosion and separated into 10 cohorts
578 consisting of 10 flies (100 total) for each genotype. Flies were maintained at 25°C and
579 transferred to fresh food every three days. For the climbing assay, each cohort was transferred
580 to 10ml serological pipette, and allowed to acclimatize for five min. For each trial, flies were
581 tapped down to the bottom of the vial, and the percentage of flies able to cross a five-ml mark
582 successfully within 10 seconds was recorded as the climbing index. Five trials were performed
583 for each cohort, with a 1-min recovery period between each trial. Climbing assays were
584 performed 10 days after eclosion.

585 **Drosophila larval injections**

586 Injections were performed by using the Nanoliter 2000 (World Precision Instruments,
587 Hertfordshire, United Kingdom) mounted on a micromanipulator (Narishige, London, United
588 Kingdom). Micropipettes were pulled from glass capillary tubes (1.14 mm OD, 0.530 mm ±
589 25 µm ID; #4878, WPI) using a laser-based micropipette puller (Sutter P-2000, Sutter
590 Instrument, Novato, CA, USA). Third instar larvae (wandering stage) were transferred to an
591 adhesive surface after being quickly washed with water to remove food residues and gently
592 dried using paper tissue. The micropipette was positioned over the approximate centre of the
593 body, on the dorsal side, and the tip was advanced through the cuticle into the hemocoel of the
594 larva. Larvae were injected with 69 nL of PBS (phosphate-buffered saline) supplemented with
595 10% (v/v) filtered food dye (PME, moss green food colouring; 0.2 µm filter). Food dye was
596 included to aid in monitoring the success of the injection under a dissection microscope (Leica
597 MZ65, Milton Keynes, United Kingdom). ω -hexatoxin-Hv1a (Hv1a, Syngenta,
598 Schaffhauserstrasse, CH-4332 Stein, Switzerland) and α -Bungarotoxin α -Btx (ab120542,
599 Abcam, Cambridge, United Kingdom) were added to the injection mix in order to obtain a final
600 concentration of 2.5 nmol/g and 1.25 nmol/g, respectively (average larval weight was 2.14 mg).
601 After injection, larvae were then gently transferred into agar/grape juice (Ritchie Products
602 Limited, Burton-On-Trent, United Kingdom) plates and kept at 25°C. The rate of survival
603 (expressed as percentage) was calculated as the number of living pupae, formed 1-2 days after
604 injection, divided by the total number of injected larvae. Experiments were repeated three times
605 independently with a total number of 10 larvae for each experimental group. Results were

606 analysed with One-way ANOVA followed by Bonferroni's multiple comparisons test using
607 GraphPad Prism (version 7, GraphPad Software, San Diego, California, USA).

608 **Coupling procedure of α -Bungarotoxin to affinity beads**

609 Coupling of α -Bungarotoxin, α -Btx (ab120542, Abcam, Cambridge, United Kingdom) to
610 cyanogen bromide-activated (CNBr) sepharose beads 4B (C9 142-5G, Sigma-Aldrich,
611 Haverhill, United Kingdom) was performed as described (Wang et al., 2003; Mulcahy et al.,
612 2018). CNBr-activated sepharose 4B beads (0.25 g) were hydrated in 1.25 ml of 1 mM HCl for
613 1 hr at 4°C on a rotator. Beads were centrifuged for 5 min at 1500 \times g, the supernatant removed
614 and beads washed twice with 1 ml of coupling buffer (0.25 M NaHCO₃, 0.5 M NaCl, pH 8.3).
615 Beads were centrifuged for 5 min at 1500 \times g and the supernatant was removed. Alpha-Btx (1
616 mg) was resuspended in 1 ml coupling buffer and incubated together with the affinity beads at
617 4°C for 16 hr on a rotator. Beads were centrifuged for 5 min at 1500 \times g. Coupling efficiency
618 was determined using a PierceTM quantitative fluorometric peptide kit and used according to
619 the manufacturer's instructions (23290, Thermo ScientificTM, Bishop's Stortford, United
620 Kingdom). Beads were blocked with 1 ml of 0.2 M glycine in 80 % coupling buffer at 4°C for
621 16 hr on a rotator. Beads were then centrifuged for 5 min at 1500 \times g and washed with 1 ml of
622 0.1 M NaHCO₃, 0.5 M NaCl, pH 8.0. This step was repeated with 1 ml of 0.1 M NaCH₃CO₂,
623 0.5 M NaCl, pH 4.0. Beads were washed again in 1 ml of 0.1 M NaHCO₃, 0.5 M NaCl, pH 8.0.
624 After a final wash step with 1 ml coupling buffer the beads were incubated twice for 30 min in
625 1 ml Tris-buffer (50 mM Tris, 150 mM NaCl, pH 8.0). The beads were centrifuged for 5 min
626 at 1500 \times g, the supernatant was removed and 20 μ l Tris-buffer, pH 8.0 was added.

627 **Membrane protein enrichment and incorporation in SMALPs**

628 *D. melanogaster* heads were obtained and separated according to (Depner et al., 2014). In a 50
629 ml falcon tube approximately 6 g flies were rapidly frozen in liquid nitrogen and vortexed twice
630 for 3 min, with the tube cooled for 30 sec in liquid nitrogen between. Heads were separated
631 from bodies by sieving (1201124 & 1201125, Endecotts, London, United Kingdom). 1 ml of
632 isotonic lysis buffer (0.25 M sucrose, 50 mM TRIS/HCl pH 7.4, 10 mM HEPES pH 7.4, 2 mM
633 EDTA, Protease inhibitor) was added to approximately 0.8 g separated heads. The solution was
634 mixed three times by vortexing and the heads were lysed with 60 strokes in a Dounce
635 homogenizer with a pestle. Membrane protein preparation was performed by differential
636 centrifugation-based fractionation as described (Depner et al., 2014; Geladaki et al., 2019).

637 Membrane protein pellets were resuspended in 20 to 100 μ l 5 % SMALP solution (5 % styrene
638 maleic acid copolymer (3:1), 5 mM Tris-Base, 0.15 mM NaCl, pH 8.0). For efficient
639 incorporation and formation of SMALPs, membrane proteins were incubated with 5 % SMALP
640 solution for 2 hr at room temperature on a rocking platform. To separate the insoluble proteins
641 from the soluble SMALPs a centrifugation step at 100000 \times g for 60 min, 4°C was performed.
642 Supernatant containing the SMALPs was combined and used for the nAChRs pull-downs.

643 **Enrichment of nAChRs by α -Btx pull-down**

644 SMALPs (20-35 mg/ml) were incubated with 200 μ l α -Btx conjugated affinity beads for 16 hr,
645 4°C on a rotator. The beads were then centrifuged for 5 min at 1500 \times g and washed two or
646 three times, each for 10 min with 1 ml ice-cold TBS (50 mM Tris, 150 mM NaCl, pH 8.0) on
647 a rotator at 4°C. Beads were centrifuged for 5 min at 1500 \times g and nAChRs selectively eluted
648 twice with 100 μ l 1 M carbachol (CAS 51-83-2, Insight Biotechnology Ltd, Wembley, United
649 Kingdom). These steps were performed for 25 min at room temperature on a rotator. Beads
650 were centrifuged for 5 min at 1500 \times g and eluates were combined and ice-cold 100 % acetone
651 in the volume of four times of the sample was added to the samples, mixed by vortexing and
652 proteins were precipitated for 16 hr at -20°C. Samples were centrifuged at 13000 \times g for 15
653 min. Supernatant was removed and dried proteins were dissolved in Laemmli buffer (1M Tris
654 pH 6.8, 10 % SDS, 5 % glycerol, 2 % bromophenol blue). Proteins were heated at 60°C and
655 loaded on Mini-Protean TGX precast gels (456–1084, 4-15 %, Bio-Rad Laboratories, Inc.,
656 Watford, United Kingdom).

657 **Electron microscopy preparation**

658 For negative staining analysis, membrane proteins were extracted with 5 % SMA and nAChRs
659 were enriched using α -Btx affinity pull-downs. Proteins were diluted 1:10 with deionised water
660 to approximately 0.9 mg/ml and an aliquot of the samples were absorbed onto a glow-
661 discharged copper/carbon-film grid (EM Resolutions) for approximately 2 min at room
662 temperature. Grids were rinsed twice in deionised water and negative staining was performed
663 using a 2 % aqueous uranyl acetate solution. Samples were viewed in a Tecnai G2 transmission
664 electron microscope (TEM, FEI/ThermoFisher) run at 200 keV accelerating voltage using a 20
665 μ m objective aperture to increase contrast; images were captured using an AMT CCD camera.

666

667 **Sample preparation for liquid chromatography–mass spectrometry (LC-MS)**

668 The protein lanes were excised from the gels and proteolytic digestion with trypsin/lys-C mix
669 (V5073, Promega, Southampton, United Kingdom) was performed as described (Shevchenko
670 et al., 2007). The gel pieces were covered with 50 mM NH₄HCO₃ / 50 % ACN and shaken for
671 10 min. This step was repeated with 100 % acetonitrile and finally dried in a speed vac. Samples
672 were reduced with 10 mM DTT in 50 mM NH₄HCO₃ at 56°C for 1 hr and alkylated with 50
673 mM iodoacetamide in 50mM NH₄HCO₃ at room temperature without light for 45 min. The gels
674 were covered with 50 mM NH₄HCO₃ and 100 % ACN and shaken for 10 min. These steps were
675 repeated and samples were dried in a speed vac. Trypsin/lys-C buffer was added to the sample
676 according to manufacturer's instructions and incubated for 45 min on ice. Next 30 µl 25 mM
677 NH₄HCO₃ was added and samples were incubated at 37°C for 16 hr. The gel pieces were
678 covered with 20 mM NH₄HCO₃ and shaken for 10 min. Supernatant with peptides was
679 collected. Next, the gels were covered with 50 % ACN / 5 % FA and shaken for 20 min. These
680 steps were repeated and peptides were dried in a speed vac. Samples for glycopeptide
681 enrichment were digested in-solution according to (Queiroz et al., 2019). Samples were
682 reduced and alkylated in 10 mM DTT and 50 mM iodoacetamide. Proteins were digested in
683 final concentration of 2.5 µg trypsin/lys-C buffer for 16 hr at 37°C.

684 **Peptide clean-up**

685 Peptides were desalted using C-18 stage tips according to (Rappaport et al., 2007). C-18
686 material (three C-18 plugs were pasted in a 200 µl pipette tip, PierceTM C18 Spin Tips, 84850
687 Thermo ScientificTM, Bishop's Stortford, United Kingdom) was equilibrated with methanol/0.1
688 % FA , 70 % ACN/0.1 % FA and with 0.1 % FA. Peptides were loaded on C-18 material,
689 washed with 0.1 % FA and eluted with 70 % ACN/0.1 % FA. Samples were dried and finally,
690 peptides were resuspended in 20 µl 0.1 % FA. For glycopeptide enrichment peptides were first
691 desalted using poros oligo r3 resin (1-339-09, Thermo ScientificTM, Bishop's Stortford, United
692 Kingdom) as described (Gobom et al., 1999; Queiroz et al., 2019). PierceTM centrifuge columns
693 (SH253723, Thermo ScientificTM, Bishop's Stortford, United Kingdom) were filled with 250 µl
694 of poros oligo r3 resin. Columns were washed three times with 0.1 % TFA. Peptides were
695 loaded onto the columns and washed three times with 0.1 % TFA and subsequently eluted with
696 70 % ACN.

697

698 **Glycopeptide enrichment**

699 Enrichment of glycopeptides of nAChRs was performed as described (Hägglund et al., 2004).
700 Micro columns were prepared with 200 μ l peptide tips filled with a C8 plug and iHILIC –
701 fusion 5 μ m, 100 Å silica based material (HCS 160119, Hilicon, Umeå, Sweden). Peptides were
702 solubilized stepwise in 19 μ l dH₂O and then in 80 μ l ACN plus 1 μ l TFA acid. The micro
703 columns were cleaned with 50 μ l 0.1 % TFA and three times equilibrated with 100 μ l 80 %
704 ACN, 1 % TFA. Peptides were loaded onto the micro column and washed twice with 100 μ l
705 80 % ACN, 1 % TFA. Glycopeptides were eluted from the column using twice 40 μ l 0.1 %
706 TFA and finally with 20 μ l 80 % ACN, 1 % TFA. Samples were dried in a speed vac before
707 peptides were deglycosylated with Endo H or PNGase F according to manufacturer's
708 instructions (P07025 & P0710S, New England Biolabs Inc., Hitchin, United Kingdom).

709 **LC-MS/MS**

710 Peptide samples were dissolved in 20 μ l of 0.1 % (v/v) FA. Approximately 1 μ g peptide
711 solution was used for each LC-MS/MS analysis. All LC-MS/MS experiments were performed
712 using a Dionex Ultimate 3000 RSLC nanoUPLC (Thermo Fisher Scientific Inc, Waltham, MA,
713 USA) system and a Q ExactiveTM Orbitrap mass spectrometer (Thermo Fisher Scientific Inc,
714 Waltham, MA, USA). Separation of peptides was performed by reverse-phase chromatography
715 at a flow rate of 300 nL/min and a Thermo Scientific reverse-phase nano Easy-spray column
716 (Thermo Scientific PepMap C18, 2 μ m particle size, 100A pore size, 75 μ m i.d. x 50 cm length).
717 Peptides were loaded onto a pre-column (Thermo Scientific PepMap 100 C18, 5 μ m particle
718 size, 100A pore size, 300 μ m i.d. x 5mm length) from the Ultimate 3000 autosampler with 0.1
719 % FA for 3 min at a flow rate of 15 μ L/min. After this period, the column valve was switched
720 to allow elution of peptides from the pre-column onto the analytical column. Solvent A was
721 water + 0.1 % FA and solvent B was 80 % ACN, 20 % water + 0.1 % FA. The linear gradient
722 employed was 2-40 % B in 90 min (the total run time including column washing and re-
723 equilibration was 120 min). In between runs columns were washed at least four times to avoid
724 any carryovers. The LC eluant was sprayed into the mass spectrometer by means of an Easy-
725 spray source (Thermo Fisher Scientific Inc.). An electrospray voltage of 2.1 kV was applied in
726 order to ionize the eluant. All m/z values of eluting ions were measured in an Orbitrap mass
727 analyzer, set at a resolution of 35000 and scanned between m/z 380-1500 Data dependent scans
728 (Top 20) were employed to automatically isolate and generate fragment ions by higher energy
729 collisional dissociation (HCD, Normalised collision energy (NCE): 25 %) in the HCD collision

730 cell and measurement of the resulting fragment ions were performed in the Orbitrap analyser,
731 set at a resolution of 17500. Singly charged ions and ions with unassigned charge states were
732 excluded from being selected for MS/MS and a dynamic exclusion of 20 seconds was
733 employed.

734 **Peptide/protein database searching**

735 Protein identification was carried out using sequest HT or mascot search engine software
736 operating in Proteome Discoverer 2.3 (Eng et al., 1994; Koenig et al., 2008). Raw flies were
737 searched against the uniprot *Drosophila_melanogaster_20180813* database (23297 sequences;
738 16110808 residues) and a common contaminant sequences database. The search parameters
739 using mascot algorithm were: (i) trypsin was set as the enzyme of choice, (ii) precursor ion
740 mass tolerance 20 ppm, (iii) fragment ion mass tolerance 0.1 Da, (iv) maximum of two missed
741 cleavage sites were set, (v) a minimum peptide length of six amino acids were set, (vi) fixed
742 cysteine static modification by carbamidomethylation, (vii) variable modification by
743 methionine oxidation & deamidation on asparagine and glutamine and N-acetylhexosamine
744 (HexNAc(1)dHex(1) + HexNAc on asparagine) as variable glycopeptide modifications, (viii)
745 A site probability threshold of 75 % was set, (ix) Percolator was used to assess the false
746 discovery rate and peptide filters were set to high confidence (FDR<1).

747 **Data handling and statistical analysis**

748 Protein data evaluation was performed using R 3.5.3 (Ihaka & Gentleman, 1996). Plotting of
749 graphs were performed in RStudio 1.3.959 (Rstudio, 2020) using ggplot2 (Ginestet, 2011) and
750 other R packages. In order to characterise membrane proteins the following tools were used:
751 (i) TMHMM - 2.0 (Krogh et al., 2001), (ii) PRED-TMBB2 (Tsirigos et al., 2016) (iii)
752 SwissPalm (Blanc et al., 2015), (iv) PredGPI (Pierleoni et al., 2008), (v) Gravy calculator
753 (www.gravy-calculator.de), (vi) Myristoylator (Bologna et al., 2004) (vii) Solubility scores
754 (Sormanni et al., 2015; Sormanni et al., 2017). Analysis of gene ontology (GO) slim terms (The
755 Gene Ontology Consortium 2019) were performed within proteome discoverer 2.3 (Thermo
756 Fisher Scientific). KEGG (Kanehisa et al., 2020) pathway enrichment analysis was performed
757 using DAVID (Huang et al., 2009). For each experimental investigation $n \geq 3$ were considered
758 and data are represented as means \pm SEM. Experiments were performed in a blinded manner
759 whenever possible. Data are presented as mean \pm SD. Statistical tests for SMALPs were
760 performed using two-tailed t-test with an unequal variance and P values of ≤ 0.05 were
761 considered to be significant. In DAVID, Fisher's exact P values are computed to measure the

762 gene-enrichment terms. Fisher's exact *P* value of 0 represents perfect enrichment of a term.
763 Usually *P* value of ≤ 0.05 are to be considered as strongly enriched. In this study the default
764 threshold set in DAVID of 0.1 was used. Linear regression analysis was performed in order to
765 study the efficiency of SMALPs extraction of membrane receptors.

766 **Structural assessment and illustration of nAChR subunits**

767 For structural alignment of nAChRs matchmaker command operating in UCSF Chimera X 0.91
768 (Goddard et al., 2018) was used. This command is superimposing protein structures by first
769 creating pairwise sequence alignments, then fitting the aligned residue pairs and displays in an
770 overlaid structure as a result. The following parameters were set to create the aligned structure:
771 (i) alignment algorithm; Needleman-Wunsch (ii) similarity matrix; BLOSUM-62. Structural
772 animation was performed in Blender 2.8 (www.blender.org), an open-source 3D graphics
773 software. For annotation of protein sequences InterProScan was used (Mitchell et al., 2019).
774 Illustrator for biological sequences (IBS) web server was used to present biological sequences
775 (Liu et al., 2015). Multiple sequence alignments were performed (Madeira et al., 2019) or using
776 BoxShade multiple sequence alignments (Swiss institute of bioinformatics).

777 **Acknowledgements**

778

779 We thank Professor Tim Dafforn for kindly providing us styrene maleic acid (SMA)
780 copolymer, Dr. Daniel Nightingale for helpful exchange and Mrs Renata Feret for technical
781 discussions. We are very grateful to Syngenta and the Milner Therapeutics Institute for
782 excellent infrastructural support. Electron microscopy was performed using the facilities at
783 CAIC (Cambridge Advanced Imaging Centre, University of Cambridge). Funding was
784 provided by BBSRC (BB/P021107/1) and Syngenta.

785 **Author Contributions**

786 Conceptualization, BD, DK, CNGG, LC, FGE, SR, and KSL; Methodology, DK, BD, CNGG,
787 RMLQ, GJ, MJD, DPM, and KHM; Data examination, BD, DK, CNGG, LCF, RMLQ, and
788 DPM; Manuscript preparation, BD, DK, CNGG, LCF, FE, SR, and KSL, with contributions of
789 all authors.

790 **Conflict of interest**

791 The authors declare no conflict of interests.

792 **Data availability**

793

794 The mass spectrometry data from this publication have been deposited to PRIDE
795 (<http://www.ebi.ac.uk/pride/archive/>) with the data set identifier PXD028484. Biochemical
796 source data is provided (Biochemical_source_data.xls).

797 **Reference**

798 Alexander JK, Govind AP, Drisdel RC, Blanton MP, Vallejo Y, Lam TT, Green WN (2010)

799 **Palmitoylation of nicotinic acetylcholine receptors** *J Mol Neurosci* **40**:12-40. DOI:
800 [10.1007/s12031-009-9246-z](https://doi.org/10.1007/s12031-009-9246-z)

801 Barnstedt O, Owald D, Felsenberg J, Brain R, Moszynski JP, Talbot CB, Perrat PN, Waddell
802 **S (2016) Memory-Relevant Mushroom Body Output Synapses Are Cholinergic**
803 *Neuron* **89**:1237–1247. DOI: [10.1016/j.neuron.2016.02.015](https://doi.org/10.1016/j.neuron.2016.02.015)

804 Blanc M, David F, Abrami L, Migliozzi D, Armand F, Bürgi J, van der Goot FG (2015)
805 **SwissPalm: Protein Palmitoylation database** *F1000Research* **4**:261. DOI:
806 [10.12688/f1000research.6464.1](https://doi.org/10.12688/f1000research.6464.1)

807 Bologna G, Yvon C, Duvaud S, Veuthey AL (2004) **N-terminal myristoylation predictions**
808 **by ensembles of neural networks** *Proteomics* **4**:1626-1632. DOI:
809 [10.1002/pmic.200300783](https://doi.org/10.1002/pmic.200300783)

810 Chambers C, Cutler P, Huang YH, Goodchild JA, Blythe J, Wang CK, Bigot A, Kaas Q,
811 Craik DJ, Sabbadin D, Earley GF (2019) **Insecticidal spider toxins are high affinity**
812 **positive allosteric modulators of the nicotinic acetylcholine receptor** *FEBS Lett*
813 **593**:1336-1350. DOI: [10.1002/1873-3468.13435](https://doi.org/10.1002/1873-3468.13435)

814 Cheng H, Fan C, Zhang SW, Wu ZS, Cui ZC, Melcher K, Zhang CH, Jiang Y, Cong Y, Xu
815 **HE (2015) Crystallization scale purification of $\alpha 7$ nicotinic acetylcholine receptor**
816 **from mammalian cells using a BacMam expression system** *Acta Pharmacol Sin*
817 **36**:1013-1023. DOI: [10.1038/aps.2015.34](https://doi.org/10.1038/aps.2015.34)

818 Dacosta CJB, Dey L, Therien JPD, Baenziger JE (2013) **A distinct mechanism for**
819 **activating uncoupled nicotinic acetylcholine receptors** *Nat Chem Biol* **9**:701-707.
820 DOI: [10.1038/nchembio.1338](https://doi.org/10.1038/nchembio.1338)

821 Dacosta CJB, Free CR, Sine SM (2015) **Stoichiometry for α -bungarotoxin block of $\alpha 7$**
822 **acetylcholine receptors** *Nat Commun* **6**:8057. DOI: [10.1038/ncomms9057](https://doi.org/10.1038/ncomms9057)

823 Dellisanti CD, Yao Y, Stroud JC, Wang ZZ, Chen L (2007) **Crystal structure of the**
824 **extracellular domain of nAChR $\alpha 1$ bound to α -bungarotoxin at 1.94 Å resolution**
825 *Nat Neurosci* **10**:953-962. DOI: [10.1038/nn1942](https://doi.org/10.1038/nn1942)

826 Denisov IG & Sligar SG (2016) **Nanodiscs for structural and functional studies of**
827 **membrane proteins** *Nat Struct Mol Biol* **23**:481-486. DOI: [10.1038/nsmb.3195](https://doi.org/10.1038/nsmb.3195)

828 Depner H, Lützkendorf J, Babkir HA, Sigrist SJ, Holt MG (2014) **Differential**
829 **centrifugation-based biochemical fractionation of the *Drosophila* adult CNS** *Nat*
830 *Protoc* **9**:2796-2808. DOI: [10.1038/nprot.2014.192](https://doi.org/10.1038/nprot.2014.192)

831 Eng JK, McCormack AL, Yates JR (1994) **An approach to correlate tandem mass spectral**

832 **data of peptides with amino acid sequences in a protein database *J Am Soc Mass***
833 ***Spectrom* **5**:976-989. DOI: [10.1016/1044-0305\(94\)80016-2](https://doi.org/10.1016/1044-0305(94)80016-2)**

834 Fang P, Ji Y, Silbern I, Doebele C, Ninov M, Lenz C, Oellerich T, Pan KT, Urlaub H (2020)
835 **A streamlined pipeline for multiplexed quantitative site-specific N-glycoproteomics**
836 *Nat Commun* **11**:5268. DOI: [10.1038/s41467-020-19052-w](https://doi.org/10.1038/s41467-020-19052-w)

837 Fayyazuddin A, Zaheer MA, Hiesinger PR, Bellen HJ (2006) **The Nicotinic Acetylcholine**
838 **Receptor Da7 Is Required for an Escape Behavior in *Drosophila*** *PLoS Biol* **4**:e63.
839 DOI: [10.1371/journal.pbio.0040063](https://doi.org/10.1371/journal.pbio.0040063)

840 Gault J, Liko I, Landreh M, Shutin D, Bolla JR, Jefferies D, Agasid M, Yen HY, Ladds
841 MJGW, Lane DP, Khalid S, Mullen C, Remes PM, Huguet R, McAlister G, Goodwin
842 M, Viner R, Syka JEP, Robinson CV (2020) **Combining native and ‘omics’ mass**
843 **spectrometry to identify endogenous ligands bound to membrane proteins** *Nat*
844 *Methods* **17**:505-508. DOI: [10.1038/s41592-020-0821-0](https://doi.org/10.1038/s41592-020-0821-0)

845 Geladaki A, Britovšek NK, Breckels LM, Smith TS, Vennard OL, Mulvey CM, Crook OM,
846 Gatto L, Lilley KS (2019) **Combining LOPIT with differential ultracentrifugation**
847 **for high-resolution spatial proteomics** *Nat Commun* **10**:331. DOI: [10.1038/s41467-018-08191-w](https://doi.org/10.1038/s41467-018-08191-w)

849 Ginestet C (2011) **ggplot2: elegant graphics for data analysis.** In *ggplot2: elegant graphics*
850 **for data analysis**, Wickham H (ed), 2nd edn, pp 1-245. New York, NY: Springer-Verlag.

851 Gobom J, Nordhoff E, Mirgorodskaya E, Ekman R, Roepstorff P (1999) **Sample**
852 **purification and preparation technique based on nano-scale reversed-phase**
853 **columns for the sensitive analysis of complex peptide mixtures by matrix-assisted**
854 **laser desorption/ionization mass spectrometry** *J Mass Spectrom* **34**:105-116. DOI:
855 [10.1002/\(SICI\)1096-9888\(199902\)34:2<105::AID-JMS768>3.0.CO;2-4](https://doi.org/10.1002/(SICI)1096-9888(199902)34:2<105::AID-JMS768>3.0.CO;2-4)

856 Goddard TD, Huang CC, Meng EC, Pettersen EF, Couch GS, Morris JH, Ferrin TE (2018)
857 **UCSF ChimeraX: Meeting modern challenges in visualization and analysis** *Protein*
858 *Sci* **27**:14-25. DOI: [10.1002/pro.3235](https://doi.org/10.1002/pro.3235)

859 Hägglund P, Bunkenborg J, Elortza F, Jensen ON, Roepstorff P (2004) **A new strategy for**
860 **identification of N-glycosylated proteins and unambiguous assignment of their**
861 **glycosylation sites using HILIC enrichment and partial deglycosylation** *J Proteome*
862 *Res* **3**:556-566. DOI: [10.1021/pr034112b](https://doi.org/10.1021/pr034112b)

863 Houchat JN, Dissanamossi BM, Landagaray E, Mathé-Allainmat M, Cartereau A, Graton J,
864 Lebreton J, Le Questel JY, Thany SH (2019) **Mode of action of sulfoxaflor on α -**
865 **bungarotoxin-insensitive nAChR1 and nAChR2 subtypes: Inhibitory effect of**
866 **imidacloprid** *Neurotoxicology* **74**:132-138. DOI: [10.1016/j.neuro.2019.06.003](https://doi.org/10.1016/j.neuro.2019.06.003)

867 Huang DW, Sherman BT, Lempicki RA (2009) **Systematic and integrative analysis of**
868 **large gene lists using DAVID bioinformatics resources** *Nat Protoc* **4**:44-57. DOI:
869 [10.1038/nprot.2008.211](https://doi.org/10.1038/nprot.2008.211)

870 Ihaka R & Gentleman R (1996) **R: A Language for Data Analysis and Graphics.** *J Comput*
871 *Graph Stat* **5**:299-314.

872 Ihara M, Furutani S, Shigetou S, Shimada S, Niki K, Komori Y, Kamiya M, Koizumi W,
873 Magara L, Hikida M, Noguchi A, Okuhara D, Yoshinari Y, Kondo S, Tanimoto H, Niwa
874 R, Sattelle DB, Matsuda K (2020) **Cofactor-enabled functional expression of fruit fly,**

875 honeybee, and bumblebee nicotinic receptors reveals picomolar neonicotinoid
876 actions *Proc Natl Acad Sci USA* **117**:16283-16291. DOI: [10.1073/pnas.2003667117](https://doi.org/10.1073/pnas.2003667117)

877 Jones AK, Davis P, Hodgkin J, Sattelle DB (2007) **The nicotinic acetylcholine receptor**
878 **gene family of the nematode *Caenorhabditis elegans*: An update on nomenclature**
879 *Invert Neurosci* **7**:129-131. DOI: [10.1007/s10158-007-0049-z](https://doi.org/10.1007/s10158-007-0049-z)

880 Kaji H, Kamiie JI, Kawakami H, Kido K, Yamauchi Y, Shinkawa T, Taoka M, Takahashi N,
881 Isobe T (2007) **Proteomics reveals n-linked glycoprotein diversity in *Caenorhabditis***
882 ***elegans* and suggests an atypical translocation mechanism for integral membrane**
883 **proteins** *Mol Cell Proteomics* **6**:2100-2109. DOI: [10.1074/mcp.M600392-MCP200](https://doi.org/10.1074/mcp.M600392-MCP200)

884 Kalxdorf M, Günthner I, Becher I, Kurzawa N, Knecht S, Savitski MM, Eberl HC,
885 Bantscheff M (2021) **Cell surface thermal proteome profiling tracks perturbations**
886 **and drug targets on the plasma membrane** *Nat Methods* **18**:84-91. DOI:
887 [10.1038/s41592-020-01022-1](https://doi.org/10.1038/s41592-020-01022-1)

888 Kanehisa M, Furumichi M, Sato Y, Ishiguro-Watanabe M, Tanabe M (2020) **KEGG:**
889 **integrating viruses and cellular organisms** *Nucleic Acids Res* **49**:D545-D551. DOI:
890 [10.1093/nar/gkaa970](https://doi.org/10.1093/nar/gkaa970)

891 Koenig T, Menze BH, Kirchner M, Monigatti F, Parker KC, Patterson T, Steen JJ,
892 Hamprecht FA, Steen H (2008) **Robust prediction of the MASCOT score for an**
893 **improved quality assessment in mass spectrometric proteomics** *J Proteome Res*
894 **7**:3708-3717. DOI: [10.1021/pr700859x](https://doi.org/10.1021/pr700859x)

895 Kondo S, Takahashi T, Yamagata N, Imanishi Y, Katow H, Hiramatsu S, Lynn K, Abe A,
896 Kumaraswamy A, Tanimoto H (2020) **Neurochemical Organization of the *Drosophila***
897 **Brain Visualized by Endogenously Tagged Neurotransmitter Receptors** *Cell Rep*
898 **30**:284-297.e5. DOI: [10.1016/j.celrep.2019.12.018](https://doi.org/10.1016/j.celrep.2019.12.018)

899 Korona D, Koestler SA, Russell S (2017) **Engineering the *Drosophila* Genome for**
900 **Developmental Biology** *J Dev Biol* **5**:16. DOI: [10.3390/jdb5040016](https://doi.org/10.3390/jdb5040016)

901 Korona D, Nightingale D, Fabre B, Nelson M, Fischer B, Johnson G, Lees J, Hubbard S,
902 Lilley K, Russell S (2020) **Characterisation of protein isoforms encoded by the**
903 ***Drosophila* Glycogen Synthase kinase 3 gene shaggy** *PLoS One* **15**:e0236679. DOI:
904 [10.1371/journal.pone.0236679](https://doi.org/10.1371/journal.pone.0236679)

905 Krogh A, Larsson B, Von Heijne G, Sonnhammer ELL (2001) **Predicting transmembrane**
906 **protein topology with a hidden Markov model: Application to complete genomes** *J*
907 *Mol Biol* **305**:567-580. DOI: [10.1006/jmbi.2000.4315](https://doi.org/10.1006/jmbi.2000.4315)

908 Lansdell SJ, Collins T, Goodchild J, Millar NS (2012) **The *Drosophila* nicotinic**
909 **acetylcholine receptor subunits Da5 and Da7 form functional homomeric and**
910 **heteromeric ion channels** *BMC Neurosci* **13**:73. DOI: [10.1186/1471-2202-13-73](https://doi.org/10.1186/1471-2202-13-73)

911 Lansdell SJ & Millar NS (2004) **Molecular characterization of Da6 and Da7 nicotinic**
912 **acetylcholine receptor subunits from *Drosophila*: Formation of a high-affinity α -**
913 **bungarotoxin binding site revealed by expression of subunit chimeras** *J Neurochem*
914 **90**:479-489. DOI: [10.1111/j.1471-4159.2004.02499.x](https://doi.org/10.1111/j.1471-4159.2004.02499.x)

915 Lee SC, Knowles TJ, Postis VLG, Jamshad M, Parslow RA, Lin YP, Goldman A, Sridhar P,
916 Overduin M, Muench SP, Dafforn TR (2016) **A method for detergent-free isolation of**
917 **membrane proteins in their local lipid environment** *Nat Protoc* **11**:1149–1162. DOI:

918 [10.1038/nprot.2016.070](https://doi.org/10.1038/nprot.2016.070)

919 Liu MY & Casida JE (1993) **High affinity binding of [3h]imidacloprid in the insect**
920 **acetylcholine receptor** *Pestic Biochem Physiol* **46**:40-46. DOI: [10.1006/pest.1993.1034](https://doi.org/10.1006/pest.1993.1034)

921 Liu W, Xie Y, Ma J, Luo X, Nie P, Zuo Z, Lahrmann U, Zhao Q, Zheng Y, Zhao Y, Xue Y,
922 Ren J (2015) **IBS: An illustrator for the presentation and visualization of biological**
923 **sequences** *Bioinformatics* **31**:3359-3361. DOI: [10.1093/bioinformatics/btv362](https://doi.org/10.1093/bioinformatics/btv362)

924 Loo RR, Dales N, Andrews PC (1996) **The effect of detergents on proteins analyzed by**
925 **electrospray ionization** *Methods Mol Biol* **61**:141-160. DOI: [10.1385/0-89603-345-7:141](https://doi.org/10.1385/0-89603-345-7:141)

927 Madeira F, Park YM, Lee J, Buso N, Gur T, Madhusoodanan N, Basutkar P, Tivey ARN,
928 Potter SC, Finn RD, Lopez R (2019) **The EMBL-EBI search and sequence analysis**
929 **tools APIs in 2019** *Nucleic Acids Res* **47**:W636-W641. DOI: [10.1093/nar/gkz268](https://doi.org/10.1093/nar/gkz268)

930 Maldonado-Hernández R, Quesada O, Colón-Sáez JO, Lasalde-Dominicci JA (2020)
931 **Sequential purification and characterization of *Torpedo californica* nAChR-DC**
932 **supplemented with CHS for high-resolution crystallization studies** *Anal Biochem*
933 **610**:113887. DOI: [10.1016/j.ab.2020.113887](https://doi.org/10.1016/j.ab.2020.113887)

934 Martens C, Shekhar M, Borysik AJ, Lau AM, Reading E, Tajkhorshid E, Booth PJ, Politis A
935 **(2018) Direct protein-lipid interactions shape the conformational landscape of**
936 **secondary transporters** *Nat Commun* **9**:4151. DOI: [10.1038/s41467-018-06704-1](https://doi.org/10.1038/s41467-018-06704-1)

937 Mitchell AL, Attwood TK, Babbitt PC, Blum M, Bork P, Bridge A, Brown SD, Chang HY,
938 El-Gebali S, Fraser MI, Gough J, Haft DR, Huang H, Letunic I, Lopez R, Luciani A,
939 Madeira F, Marchler-Bauer A, Mi H, Natale DA, Necci M, Nuka G, Orengo C,
940 Pandurangan AP, Paysan-Lafosse T, Pesseat S, Potter SC, Qureshi MA, Rawlings ND,
941 Redaschi N, Richardson LJ, Rivoire C, Salazar GA, Sangrador-Vegas A, Sigrist CJA,
942 Sillitoe I, Sutton GG, Thanki N, Thomas PD, Tosatto SCE, Yong SY, Finn RD (2019)
943 **InterPro in 2019: Improving coverage, classification and access to protein sequence**
944 **annotations** *Nucleic Acids Res* **47**:D351-D360. DOI: [10.1093/nar/gky1100](https://doi.org/10.1093/nar/gky1100)

945 Mulcahy MJ, Paulo JA, Hawrot E (2018) **Proteomic Investigation of Murine Neuronal $\alpha 7$ -**
946 **Nicotinic Acetylcholine Receptor Interacting Proteins** *J Proteome Res* **17**:3959-3975.
947 DOI: [10.1021/acs.jproteome.8b00618](https://doi.org/10.1021/acs.jproteome.8b00618)

948 Perry T, Chen W, Ghazali R, Yang YT, Christesen D, Martelli F, Lumb C, Luong HNB,
949 Mitchell J, Holien JK, Parker MW, Sparks TC, Batterham P (2021) **Role of nicotinic**
950 **acetylcholine receptor subunits in the mode of action of neonicotinoid, sulfoximine**
951 **and spinosyn insecticides in *Drosophila melanogaster*** *Insect Biochem Mol Biol*
952 **131**:103547. DOI: [10.1016/j.ibmb.2021.103547](https://doi.org/10.1016/j.ibmb.2021.103547)

953 Perry T, Heckel DG, McKenzie JA, Batterham P (2008) **Mutations in $\alpha 1$ or $\beta 2$ nicotinic**
954 **acetylcholine receptor subunits can confer resistance to neonicotinoids in**
955 ***Drosophila melanogaster*** *Insect Biochem Mol Biol* **38**:520-528. DOI:
956 DOI: [10.1016/j.ibmb.2007.12.007](https://doi.org/10.1016/j.ibmb.2007.12.007)

957 Perry T, Somers J, Yang YT, Batterham P (2015) **Expression of insect $\alpha 6$ -like nicotinic**
958 **acetylcholine receptors in *Drosophila melanogaster* highlights a high level of**
959 **conservation of the receptor: spinosyn interaction** *Insect Biochem Mol Biol* **64**:106-
960 115. DOI: [10.1016/j.ibmb.2015.01.017](https://doi.org/10.1016/j.ibmb.2015.01.017)

961 Pierleoni A, Martelli PL, Casadio R (2008) **PredGPI: A GPI-anchor predictor** *BMC*
962 *Bioinformatics* **9**: 392. DOI: [10.1186/1471-2105-9-392](https://doi.org/10.1186/1471-2105-9-392)

963 Queiroz RML, Smith T, Villanueva E, Marti-Solano M, Monti M, Pizzinga M, Mirea D-M,
964 Ramakrishna M, Harvey RF, Dezi V, Thomas GH, Willis AE, Lilley KS (2019)
965 **Comprehensive identification of RNA-protein interactions in any organism using**
966 **orthogonal organic phase separation (OOPS)** *Nat Biotechnol* **37**:169-178. DOI:
967 [10.1038/s41587-018-0001-2](https://doi.org/10.1038/s41587-018-0001-2)

968 Quesada O, González-Freire C, Ferrer MC, Colón-Sáez JO, Fernández-García E, Mercado J,
969 Dávila A, Morales R, Lasalde-Dominicci JA (2016) **Uncovering the lipidic basis for**
970 **the preparation of functional nicotinic acetylcholine receptor detergent complexes**
971 **for structural studies** *Sci Rep* **6**:32766. DOI: [10.1038/srep32766](https://doi.org/10.1038/srep32766)

972 Rahman MM, Teng J, Worrell BT, Noviello CM, Lee M, Karlin A, Stowell MHB, Hibbs RE
973 (2020) **Structure of the Native Muscle-type Nicotinic Receptor and Inhibition by**
974 **Snake Venom Toxins** *Neuron* **106**:952-962.e5. DOI: [10.1016/j.neuron.2020.03.012](https://doi.org/10.1016/j.neuron.2020.03.012)

975 Rappaport J, Mann M, Ishihama Y (2007) **Protocol for micro-purification, enrichment,**
976 **pre-fractionation and storage of peptides for proteomics using StageTips** *Nat*
977 *Protoc* **2**:1896–1906. DOI: [10.1038/nprot.2007.261](https://doi.org/10.1038/nprot.2007.261)

978 Rohde PD, Madsen LS, Neumann Arvidson SM, Loeschke V, Demontis D, Kristensen TN
979 (2016) **Testing candidate genes for attention-deficit/hyperactivity disorder in fruit**
980 **flies using a high throughput assay for complex behavior** *Fly (Austin)* **10**:25-34.
981 DOI: [10.1080/19336934.2016.1158365](https://doi.org/10.1080/19336934.2016.1158365)

982 Rstudio Team (2020) **RStudio: Integrated Development for R.** *Rstudio, PBC, Boston, MA*
983 URL <http://www.rstudio.com/>.

984 Salgado VL (2021) **Selective actions of insecticides on desensitizing and non-**
985 **desensitizing nicotinic acetylcholine receptors in cockroach (*Periplaneta americana*)**
986 **neurons** *Pest Manag Sci* **77**:3663-3672. DOI: [10.1002/ps.6396](https://doi.org/10.1002/ps.6396)

987 Schmidt-Nielsen BK, Gepner JI, Teng NNH, Hall LM (1977) **Characterization of an a-**
988 **bungarotoxin binding component from *Drosophila melanogaster*** *J Neurochem*
989 **29**:1013-1029. DOI: [10.1111/j.1471-4159.1977.tb06505.x](https://doi.org/10.1111/j.1471-4159.1977.tb06505.x)

990 Shevchenko A, Tomas H, Havliš J, Olsen JV, Mann M (2007) **In-gel digestion for mass**
991 **spectrometric characterization of proteins and proteomes** *Nat Protoc* **1**:2856–2860.
992 DOI: [10.1038/nprot.2006.468](https://doi.org/10.1038/nprot.2006.468)

993 Sobotzki N, Schafroth MA, Rudnicka A, Koetemann A, Marty F, Goetze S, Yamauchi Y,
994 Carreira EM, Wollscheid B (2018) **HATRIC-based identification of receptors for**
995 **orphan ligands** *Nat Commun* **9**:1519. DOI: [10.1038/s41467-018-03936-z](https://doi.org/10.1038/s41467-018-03936-z)

996 Somers J, Luong HNB, Mitchell J, Batterham P, Perry T (2017) **Pleiotropic effects of loss of**
997 **the Da1 subunit in *Drosophila melanogaster*: Implications for insecticide resistance**
998 *Genetics* **205**:263-271. DOI: [10.1534/genetics.116.195750](https://doi.org/10.1534/genetics.116.195750)

999 Sormanni P, Amery L, Ekizoglou S, Vendruscolo M, Popovic B (2017) **Rapid and accurate**
1000 **in silico solubility screening of a monoclonal antibody library** *Sci Rep* **7**:8200. DOI:
1001 [10.1038/s41598-017-07800-w](https://doi.org/10.1038/s41598-017-07800-w)

1002 Sormanni P, Aprile FA, Vendruscolo M (2015) **The CamSol method of rational design of**
1003 **protein mutants with enhanced solubility** *J Mol Biol* **427**:478-490. DOI:

1004 [10.1016/j.jmb.2014.09.026](https://doi.org/10.1016/j.jmb.2014.09.026)

1005 Su H & O'Dowd DK (2003) **Fast synaptic currents in *Drosophila* mushroom body**
1006 **kenyon cells are mediated by α -bungarotoxin-sensitive nicotinic acetylcholine**
1007 **receptors and picrotoxin-sensitive GABA receptors** *J Neurosci* **23**:9246–9253. DOI:
1008 [10.1523/JNEUROSCI.23-27-09246.2003](https://doi.org/10.1523/JNEUROSCI.23-27-09246.2003)

1009 Tackenberg MC, Giannoni-Guzmán MA, Sanchez-Perez E, Doll CA, Agosto-Rivera JL,
1010 Broadie K, Moore D, McMahon DG (2020) **Neonicotinoids disrupt circadian**
1011 **rhythms and sleep in honey bees** *Sci Rep* **10**:17929. DOI: [10.1038/s41598-020-72041-3](https://doi.org/10.1038/s41598-020-72041-3)

1013 Tsirigos KD, Elofsson A, Bagos PG (2016) **PRED-TMBB2: Improved topology prediction**
1014 **and detection of beta-barrel outer membrane proteins** *Bioinformatics* **32**:i665-i671.
1015 DOI: [10.1093/bioinformatics/btw444](https://doi.org/10.1093/bioinformatics/btw444)

1016 The Gene Ontology Consortium (2019) **The Gene Ontology Resource: 20 years and still**
1017 **GOing strong** *Nucleic Acids Res* **47**:D330-D338. DOI: [10.1093/nar/gky1055](https://doi.org/10.1093/nar/gky1055)

1018 Wang H, Yu M, Ochani M, Amella CA, Tanovic M, Susarla S, Li JH, Wang H, Yang H,
1019 Ulloa L, Al-Abed Y, Czura CJ, Tracey KJ (2003) **Nicotinic acetylcholine receptor α 7**
1020 **subunit is an essential regulator of inflammation** *Nature* **421**:384-388. DOI:
1021 [10.1038/nature01339](https://doi.org/10.1038/nature01339)

1022 Wu P, Ma D, Pierzchala M, Wu J, Yang LC, Mai X, Chang X, Schmidt-Glenewinkel T
1023 (2005) **The *Drosophila* acetylcholine receptor subunit Da5 is part of an α -**
1024 **bungarotoxin binding acetylcholine receptor** *J Biol Chem* **280**:20987-20994. DOI:
1025 [10.1074/jbc.M409639200](https://doi.org/10.1074/jbc.M409639200)

1026 Xu X, Bao H, Shao X, Zhang Y, Yao X, Liu Z, Li Z (2010) **Pharmacological**
1027 **characterization of cis-nitromethylene neonicotinoids in relation to imidacloprid**
1028 **binding sites in the brown planthopper, *Nilaparvata lugens*** *Insect Mol Biol* **19**:1-8.
1029 DOI: [10.1111/j.1365-2583.2009.00923.x](https://doi.org/10.1111/j.1365-2583.2009.00923.x)

1030 Zuo YY, Xue YX, Wang ZY, Ren X, Aioub AAA, Wu YD, Yang YH, Hu ZN (2021)
1031 **Knockin of the G275E mutation of the nicotinic acetylcholine receptor (nAChR) α 6**
1032 **confers high levels of resistance to spinosyns in *Spodoptera exigua*** *Insect Sci* **0**:1-9.
1033 DOI: [10.1111/1744-7917.12922](https://doi.org/10.1111/1744-7917.12922)

1034

1035

1036

1037

1038

1039

1040

1041

1042

1043

1044

1045

1046

1047

1048 **Appendix tables and figures supplement**

1049

1050 **Table of Contents**

1051

1052	Table 1 Climbing ability	37
1053	Table 2 <i>Drosophila</i> larval injection of ω -Hexatoxin-Hv1a & α -Bungarotoxin	38
1054	Table 3 Identified nAChR peptides in pull-downs with α -Bungarotoxin.....	38
1055	Table 4 Identified nAChR peptides in pull-downs without α -Bungarotoxin.	38
1056	Table 5 List of gRNAs and oligonucleotides used for cloning	41
1057	Table 6 List of oligonucleotides used for amplification from genomic DNA	42
1058	Table 7 C-terminal tagging of nAChRa6 with FSVS	43
1059	Figure supplement 1 GO terms and predicted membrane proteins	44
1060	Figure supplement 2 Identified peptides in ligand-binding and cytoplasmic domain	45
1061	Figure supplement 3 Superimposed nAChR α -subunits structure together with identified peptide	46
1063	Figure supplement 4 Glycosylation sites of nAChR subunits.....	47

1064

1065

1066

1067 **Table 1. Climbing ability.**

10 days old flies									
number	receptor	series 1		series 2		series 3		average	standard deviation
	subunit	percentage	actual change	percentage	actual change	percentage	actual change	percent	STEV
1	nAChR $\alpha 1$	30	37.5	40	50	50	71.4	53	17.2
2	nAChR $\alpha 2$	40	50	40	50	50	71.4	57.1	12.4
3	nAChR $\alpha 3$	0	0	20	25	30	42.9	22.6	21.5
4	nAChR $\alpha 4$	70	87.5	80	100	60	85.7	91.1	7.8
5	nAChR $\alpha 5$	60	75	70	87.5	50	71.4	78	8.4
6	nAChR $\alpha 6$	40	50	50	62.5	50	71.4	61.3	10.8
7	nAChR $\alpha 7$	70	87.5	80	100	70	100	95.8	7.2
8	nAChR $\beta 1$	30	37.5	30	37.5	20	28.6	34.5	5.2
9	nAChR $\beta 2$	80	100	80	100	60	85.7	95.2	8.2
10	nAChR $\beta 3$	80	100	80	100	70	100	100	0
11	WT	80	100	80	100	70	100	100	0

1068

1069

1070

1071 **Table 2. *Drosophila* larval injection of ω -Hexatoxin-Hv1a & α -Bungarotoxin.**

	Strain	Injected cpd	Survival (% of pupae formed after injection)				
			Rep1	Rep2	Rep3	Average	Standard Deviation
CONTROL	w ¹¹¹⁸	2.5 nmol/g Hv1a	0	0	0	0	0
CONTROL - Cas9 lines	THattP40	2.5 nmol/g Hv1a	0	0	0	0	0
CONTROL - Cas9 lines	THattP2	2.5 nmol/g Hv1a	0	0	0	0	0
nAChR CRISPR mutant	nAChR α 1	2.5 nmol/g Hv1a	25	0	0	8.33	14.43
nAChR CRISPR mutant	nAChR α 2	2.5 nmol/g Hv1a	25	0	0	8.33	14.43
nAChR CRISPR mutant	nAChR α 3	2.5 nmol/g Hv1a	0	0	0	0	0
nAChR CRISPR mutant	nAChR α 4	2.5 nmol/g Hv1a	25	33.33	66.67	41.67	22.05
nAChR CRISPR mutant	nAChR α 5	2.5 nmol/g Hv1a	0	0	0	0	0
nAChR CRISPR mutant	nAChR α 6	2.5 nmol/g Hv1a	0	0	0	0	0
nAChR CRISPR mutant	nAChR α 7	2.5 nmol/g Hv1a	0	0	0	0	0
nAChR CRISPR mutant	nAChR β 2	2.5 nmol/g Hv1a	25	33.33	66.67	41.67	22.05
nAChR CRISPR mutant	nAChR β 3	2.5 nmol/g Hv1a	0	33.33	0	11.11	19.25
Injection CONTROL	w ¹¹¹⁸	PBS	100	100	100	100	0
CONTROL	w ¹¹¹⁸	1.25 nmol/g α -Btx	0	0	0	0	0
CONTROL - Cas9 lines	THattP40	1.25 nmol/g α -Btx	0	0	0	0	0
CONTROL - Cas9 lines	THattP2	1.25 nmol/g α -Btx	0	0	0	0	0
nAChR CRISPR mutant	nAChR α 1	1.25 nmol/g α -Btx	0	0	33.33	11.11	19.25
nAChR CRISPR mutant	nAChR α 2	1.25 nmol/g α -Btx	25	0	33.33	19.44	17.35
nAChR CRISPR mutant	nAChR α 3	1.25 nmol/g α -Btx	0	0	33.33	11.11	19.25
nAChR CRISPR mutant	nAChR α 4	1.25 nmol/g α -Btx	0	33.33	0	11.11	19.25
nAChR CRISPR mutant	nAChR α 5	1.25 nmol/g α -Btx	50	66.67	66.67	61.11	9.62
nAChR CRISPR mutant	nAChR α 6	1.25 nmol/g α -Btx	25	66.67	66.67	52.78	24.06
nAChR CRISPR mutant	nAChR α 7	1.25 nmol/g α -Btx	50	100	66.67	72.22	25.46
nAChR CRISPR mutant	nAChR β 2	1.25 nmol/g α -Btx	0	33.33	0	11.11	19.25
nAChR CRISPR mutant	nAChR β 3	1.25 nmol/g α -Btx	0	0	0	0	0
Injection CONTROL	w ¹¹¹⁸	PBS	100	100	100	100	0

1072

1073 **Table 3. Identified nAChR peptides in pull-downs with α -Bungarotoxin.**

1074 Peptides from Da3, Da5, Da6, Da7 and D β 3 nAChR subunits are listed and found [N] times within
 1075 individual replicates. Protein domains are marked with: Ed extracellular-, Id Intracellular-, LBD ligand-
 1076 binding-, and Non-domain localization. The mass-to-charge ratio (m/z) of the precursor ions, the
 1077 protonated monoisotopic masses, the theoretical MH^+ masses in Dalton [Da] and peptide modifications
 1078 are listed. Peptide modifications are listed with: (C) Carbamidomethylation; (N,Q) Deamidation; (H)
 1079 N-acetylhexosamine (HexNAc); (M) Oxidation.

1080 **Table 4. Identified nAChR peptides in pull-downs without α -Bungarotoxin.**

1081 Identified peptides of nAChR subunits which are found in control pull-down samples without α -
 1082 Bungarotoxin (α -Btx).

1083

Table 3. Identified nAChR peptides in pull-downs with α -Bungarotoxin.

Subunit	Accession	Sequence	Found [N]	Domain	m/z [Da]	MH+ [Da]	Theo. MH+ [Da]	Modification
nAChR α 3	Q9W3G6	ATLnYTGR	2	LBD	549.77423	1098.54119	1098.54258	H4 or position 2 , 6
nAChR α 5	Q7KT97	TVYGQGDDGSIGPIGSTR	7	Id	890.42413	1779.84099	1779.85078	
nAChR α 5	Q7KT97	TVYGqGDDGSIGPIGSTR	2	Id	890.93036	1780.85344	1780.83480	Q5
nAChR α 5	Q7KT97	FITDQLR	7	Id	446.74768	892.48808	892.48869	
nAChR α 5	Q7KT97	KHQILSDVELKER	1	Id	399.47717	1594.8869	1594.8911	
nAChR α 5	Q7KT97	SSTEYEGLILK	1	Id	676.86945	1352.7316	1352.7308	
nAChR α 5, α 7	Q7KTF97, Q9VWI9	LEWNDMNLR	1	LBD	595.78156	1190.55583	1190.5623	
nAChR α 5, α 7	Q7KTF97, Q9VWI9	NnGScLYVPPGIFK	2	LBD	884.93384	1768.86040	1768.85745	H2, C5
nAChR α 5, α 7	Q7KTF97, Q9VWI9	NnGScLYVPPGIFK	2	LBD	783.88092	1566.75456	1566.76209	N2, C5
nAChR α 5, α 7	Q7KTF97, Q9VWI9	nnGScLYVPPGIFK	2	LBD	784.39069	1567.77410	1567.74611	N1, N2, C5
nAChR α 6	Q7KTF9	ELQFITAR	4	Id	489.27380	977.54033	977.54146	
nAChR α 6	Q7KTF9	ELqFITAR	1	Id	489.7753	978.54332	978.52547	Q3
nAChR α 6	Q7KTF9	TADIHEMPPWIK	1	Non	719.36407	1437.72087	1437.71950	
nAChR α 6	Q7KTF9	TILLSNR	4	Id	408.75095	816.49462	816.49378	
nAChR α 6	Q7KTF9	ADDEAEELIGDWK	4	Id	681.3179	1361.61.61785	1361.62195	
nAChR α 6	Q7KTF9	KADDEAEELIGDWK	1	Id	745.36469	1489.72209	1489.71691	
nAChR α 6	Q7KTF9	KTILLSNR	2	Id	472.79971	944.59215	944.58874	
nAChR α 5, α 6, α 7	Q7KT97, Q7KTF9, Q9VWI9	IDITWFPFDDQR	3	LBD	776.87292	1552.7386	1552.7431	
nAChR α 5, α 6, α 7	Q7KT97, Q7KTF9, Q9VWI9	SLLANVLDIDDDFR	3	Id	803.40924	1605.8112	1605.8119	
nAChR α 6, α 7	Q7KTF9, Q9VWI9	IDITWFPFDDQR	1	LBD	777.37311	1553.73894	1553.7209	Q11
nAChR α 7	Q9VWI9	SLLANVLDIDDDFRcNHR	1	Id	544.01544	2173.0399	2173.0455	C15
nAChR α 7	Q9VWI9	KQQIQNVELKER	6	Id	504.95410	1512.84774	1512.84927	
nAChR α 7	Q9VWI9	KQQIQNVELK	1	Id	614.35730	1227.70732	1227.70556	
nAChR α 7	Q9VWI9	KQqIQNVELKER	1	Id	502.29062	1513.8573	1513.8333	N3
nAChR α 7	Q9VWI9	QGDDGSVGPVGPAGPVVDGR	12	Id	918.44794	1835.88860	18335.88823	
nAChR α 7	Q9VWI9	qGDDGSVGPVGPAGPVVDGR	1	Id	918.94897	1936.89067	1836.87225	Q1
nAChR α 7	Q9VWI9	QQIQNVELK	1	Id	550.30487	1099.60246	1099.61060	
nAChR α 7	Q9VWI9	EDETSDTIR	1	Non	533.23535	1065.46343	1065.46947	
nAChR α 7	Q9VWI9	mQRPGQVGYEcPPPPSSSSASGEK	1	Id	908.41028	2723.2163	2723.2036	M1; C11
nAChR α 7	Q9VWI9	casATLPHQPTYYR	2	Id	555.59827	1664.7803	1664.785	C1
nAChR α 7	Q9VWI9	WITEQLKKEDETSDTIR	2	Id	698.01874	2092.0417	2092.0557	
nAChR α 7	Q9VWI9	WITEQLK	1	Non	459.25516	917.50304	917.50909	
nAChR α 7	Q9VWI9	cNHRCASATLPHQPTYYR	1	Id	832.89795	1664.7886	1664.785	C1
nAChR β 3	Q9VPQ8	VVLPEnGTAR	1	LBD	629.83380	1258.66033	1258.66376	H6 or position 8

Table 4. Identified nAChR peptides in pull-downs without α -Bungarotoxin.

Subunit	Accession	Sequence	Found [N]	Domains	m/z [Da]	MH+ [Da]	Theo. MH+ [Da]	Modification
nAChR α 1	AOA0B4KGU3	LFIQILPK	1	Ed	486.31339	971.61949	917.62882	
nAChR α 1, α 2	AOA0B4KGU3, P17644	LYDDLLSNYNR	1	Ed	693.3407	1385.674	1385.66957	
nAChR α 2	P17644	AIDVQLSDVAK	2	Non	579.823	1158.639	1158.636	
nAChR α 2	P17644	VVWTTPPAIFK	1	Ed	579.3391	1157.671	1157.671	
nAChR α 2, β 2	P17644, P25162	LSQLIEVNLIK	1	Ed	386.5676	1157.692	1157.677	
nAChR α 4	A8JNX5	LVSSGYNNNSLPK	10	Non	639.8441	1278.661	1278.66884	
nAChR α 4	A8JNX5	LVSSGYnNSLPK	1	Non	640.3381	1279.669	1279.653	N7
nAChR α 4	A8JNX5	LSQLIDVNLIK	2	LBD	571.8425	1142.678	1142.678	
nAChR α 4	A8JNX5	SPILNNPAFSHSK	1	Non	471.24591	1411.72318	1411.73284	
nAChR α 4	A8JNX5	RPTYNFETSK	3	Non	621.80939	1242.61150	1242.61133	
nAChR α 4	A8JNX5	RPTYnFETSK	3	Non	622.3102	1243.613	1243.595	N5
nAChR α 4	A8JNX5	LYDDLLSNYNK	2	LBD	679.3725	1357.64910	1357.66342	
nAChR α 4	A8JNX5	RPTYNFETSKLLLK	1	Non	621.8079	1242.609	1242.611	
nAChR β 1	P04755	NKNFVDSLSDYWK	2	Ed	643.8068	1286.600	1286.605	
nAChR β 1	P04755	NFVDSLSDYWK	4	Ed	643.8044	1286.602	1286.605	
nAChR β 1	P04755	nFVDSLSDYWK	4	Ed	644.3093	1287.611	1287.589	N1
nAChR β 1	P04755	ILPPTSVLPLIAK	1	Non	737.9825	1474.96074	1474.96071	
nAChR β 1	P04755	ATEAVEFIAEHLR	5	Id	495.92743	1485.76773	1485.76962	
nAChR β 1	P04755	VVKPDIVLFNNADGNYEVR	1	Ed	750.3779	2249.119	2249.135	
nAChR β 2	P25162	LYDDLLSNYNR	3	Ed	693.34070	1385.67412	1385.66957	
nAChR β 2	P25162	LSqLIEVNLSNqVMTTNLWVK	1	Ed	825.1133	2473.325	2473.3370	Q3; Q12
nAChR β 2	P25162	LSqLIEVNLIK	2	Ed	386.5676	1157.688	1157.678	Q3

Table 5. List of gRNAs and oligonucleotides used for cloning.

Knockouts				
nAChR subunit	gRNA target name	gRNA sequence (NGG)	oligonucleotides name (Forward/Reverse)	oligonucleotides sequence
nAChR α 1	Da1_111(+)	5'CGGAGATGTAGTAGTCCTGCAGG3'	41_Da1_111_F	5'GTCGCGGAGATGTAGTAGTCCTGC3'
			42_Da1_111_R	5'AAACGCAGGACTACTACATCTCG3'
	Da1_126(-)	5'CCTGCAGGTCGATGCCACCTCG3'	43_Da1_126_F	5'GTCGCGAGGTGGGCATCGACCTGC3'
			44_Da1_126_R	5'AAACGCAGGTCGATGCCACCTCG3'
nAChR α 2	Da2_99 (+)	5'GCTCCTCTCGAAACCGTTAGG3'	45_Da2_99_F	5'GTCGCTCTCTCGAAACCGTTAGG3'
			46_Da2_99_R	5'AAACGAACGGTTTCGACAGAGGAG3'
nAChR α 3	Da3_18(+)	5'GTCCGGACGCCAGATGTGATCGG3'	49_Da3_18_F	5'GTCGTCGGACGCCAGATGTGATCGG3'
			50_Da3_18_R	5'AAACATCACATCTGGGTCCGA3'
nAChR α 4	Da4_19(+)	5'TTGTGCGACGAACCATACTTGG3'	53_Da4_19_F	5'GTCGTTGTCGACGAACCATACTTGG3'
			54_Da4_19_R	5'AAACAGTATGGTTCGTCGCAACAA3'
nAChR α 5	Da5_232(-)	5'CCGGGGATCTCAAGTCGACGTG3'	57_Da5_232_F	5'GTCGACGTGACTGAAGATCC3'
			58_Da5_232_R	5'AAACGGGATCTCAAGTCGACGTG3'
	Da5_251(+)	5'CGTCAAGATCGACATCACGTGG3'	59_Da5_251_F	5'GTCGCGTGCAAGATCGACATCACGTG3'
			60_Da5_251_R	5'AAACCGTGATGTCGATCTGCACG3'
nAChR α 6	Da6_70(+)	5'CGTATTCTCTTCCCGGATGG3'	61_Da6_70_F	5'GTCGCGTATTCTCTTCCCGGCA3'
			62_Da6_70_R	5'AAACTGCCGGAAAGAAGAACG3'
nAChR α 7	Da7_1226(+)	5'CATTGACCACCGGACGCCAGG3'	63_Da7_1226_F	5'GTCGCATTGACCACCGGACGCCAGG3'
			64_Da7_1226_R	5'AAACGGAGCGTCCGGTGGTCAATG3'
nAChR β 1	Db1_2(+)	5'TGGAGTCTCCTGCAAATCCTGG3'	67_Db1_2_F	5'GTCGTGGAGTCTCCTGCAAATCCTGG3'
			68_Db1_2_R	5'AAACGGGATTGCAAGGAAGACTCCA3'
nAChR β 2	Db2_955(+)	5'TCAGACCTAACCAACCGTCAGG3'	71_Db2_955_F	5'GTCGTCAGACCTAACCAACCGTC3'
			72_Db2_955_R	5'AAACGACGGTTGGTTAGGTCTGA3'
nAChR β 3	Db3_466(+)	5'CTTGAAGTCCAGCGAGGTCTGG3'	75_Db3_466_F	5'GTCGCTTGAAGTCCAGCGAGGTCTGG3'
			76_Db3_466_R	5'AAACGACCTCGCTGGACTTCAAAG3'
C-terminal tagging				
nAChR subunit	gRNA target name	gRNA sequence (NGG)	oligonucleotides name (Forward/Reverse)	oligonucleotides sequence
nAChR α 6	Da6_181(+)	5'TTGCACGATTATGTGCGGAGCGG3'	131_Da6_181_F	5'GTCGTTGCACGATTATGTGCGGAGCGG3'
			132_Da6_181_R	5'AAACCTCCGCACATAATCGTGC3'
	Da6_176(+)	5'CCTTATTGACGATTATGTGCGG3'	133_Da6_176_F	5'GTCGCCTTATTGACGATTATGTGCGG3'
			134_Da6_176_R	5'AAACACATAATCGTGC3'

Table 6. List of oligonucleotides used for amplification from genomic DNA.

knockouts			
nAChR subunit	homology arm	oligonucleotides name (Forward/Reverse)	oligonucleotides sequence
nAChR α 1	Da1_LHA	Da1_LHA_F1	5'TGGGGCGACAAATAGCATG3'
		Da1_LHA_R1	5'GGGGAAATGGGCAACAAAT3'
nAChR α 1	Da1_RHA	Da1_RHA_F1	5'GCAGATACTTCCCAGCAGC3'
		Da1_RHA_R1	5'CCCGCGCTTGTACTTTG3'
nAChR α 2	Da2_LHA	Da2_LHA_F1	5'ACGAAATGCAAAACCGAGCT3'
		Da2_LHA_R2	5'CCCAATTGACCAACACCGT3'
nAChR α 2	Da2_RHA	Da2_RHA_F1	5'GCGGGCAGAAAGTAAACAA3'
		Da2_RHA_R1	5'TCACCTGATCACCGTCGTAG3'
nAChR α 3	Da3_LHA	Da3_LHA_F1	5'CTCCAGCCGTTCCCAAATCT3'
		Da3_LHA_R1	5'CAATCTGTGGTGGAGCAGT3'
nAChR α 3	Da3_RHA	Da3_RHA_F1	5'CTGCTCGTCGAAGGGAAAGT3'
		Da3_RHA_R1	5'GATCCAGCCAGACTAACGCC3'
nAChR α 4	Da4_LHA	Da4_LHA_F1	5'GATGAACAACAGGGCAGCAA3'
		Da4_LHA_R1	5'CAAAACAACAACCGTCACGC3'
nAChR α 4	Da4_RHA	Da4_RHA_F1	5'TTAGAGCGTAACAGTGGCG3'
		Da4_RHA_R1	5'ACGCCTACAAACCGGACAAA3'
nAChR α 5	Da5_LHA	Da5_LHA_F1	5'ACCGCATTCTGTCGCATAT3'
		Da5_LHA_R1	5'CAGGACGACGTTGGCTACT3'
nAChR α 5	Da5_RHA	Da5_RHA_F1	5'GGATCTTCAAGTCGACGTG3'
		Da5_RHA_R1	5'GAGGGTGTGGCTGGATTT3'
nAChR α 6	Da6_LHA	Da6_LHA_F1	5'GTGTACGGGTGTGAGACAGA3'
		Da6_LHA_R1	5'TCACACATTGCTGCCGAAA3'
nAChR α 6	Da6_RHA	Da6_RHA_F1	5'GTCAGTTCTGCCCGAAC3'
		Da6_RHA_R1	5'CCGAGAGTTGACTGTAGCCA3'
nAChR α 7	Da7_LHA	Da7_LHA_F1	5'TGTAAACCCTAGCAGTGCCA3'
		Da7_LHA_R1	5'TATGATACCGGGTGAGTGCC3'
nAChR α 7	Da7_RHA	Da7_RHA_F1	5'CATCCGGTTCCATAGGCGA3'
		Da7_RHA_R1	5'ACGAAATCACATGCCCT3'
nAChR β 1	Db1_LHA	Db1_LHA_F1	5'TCATCAACAGCAGGAGAGA3'
		Db1_LHA_R1	5'TGGCAATGAGAGCTGGAGA3'
nAChR β 1	Db1_RHA	Db1_RHA_F1	5'CTGCAAATCCTGGCTGTTGT3'
		Db1_RHA_R1	5'GTGTGTGTGTGTTGGTCT3'
nAChR β 2	Db2_LHA	Db2_LHA_F1	5'TCAACTCAGGACAGCACACA3'
		Db2_LHA_R1	5'ACCAACTTCCCTAGCTCC3'
nAChR β 2	Db2_RHA	Db2_RHA_F1	5'CCCATCGCAACTTGTAGTCG3'
		Db2_RHA_R1	5'CATTCTGTCAGGTAAGTGC3'
nAChR β 3	Db3_LHA	Db3_LHA_F1	5'AACGGTCCGATGACTTCCT3'
		Db3_LHA_R1	5'TGAGCATGTTGAGTCGAG3'
nAChR β 3	Db3_RHA	Db3_RHA_F1	5'TCCTCGTCCTCTCCTCGT3'
		Db3_RHA_R1	5'TTCTGCAGGAAACTACGACC3'

Table 6. Continued, List of oligonucleotides used for amplification from genomic DNA.

C-terminal tagging			
nAChR subunit	homology arm	oligonucleotides name (Forward/Reverse)	oligonucleotides sequence
nAChR α 6	Da6_RHA	74_Da6_RHA_F_Gen	5'GGGTTTCTGTTCTTGCCTG3'
		75_Da6_RHA_R_Gen	5'GCCCTGCTGATTTGTTGCT3'
nAChR α 6	Da6_LHA	76_Da6_LHA_F_Gen	5'CCGATGCTTCCGACGTATCC3'
		77_Da6_LHA_R_Gen	5'GCCATACTAGCGCATGACTCT3'

Table 7. C-terminal tagging of nAChR α 6 with FSVS.

C-terminal tagging with FSVS			
nAChR subunit	fragment	site	oligonucleotides sequence
nAChR α 6	31	105_Donor_LHA_Da6	5'CGGGCTAATTATGGGGTGTGCCCTGTGCATGCAGAGAATGAAACC3'
		106_LHA_Da6_linker_R	5'CCTTGCACGATTATGTGCGGAGCTGAGAGCAGCACCGTAACCG3'
	32	107_linkerTag_F	5'GCTCTCAGCTCCGACATAATCGTCAAGGATCCGGCGAGGGGC3'
		108_RHDa6_Tag_R	5'CTAATTCGAGCGTCCTACTTTCGAACTGGGGATGGC3'
	33	109_TG-RHA_Da6_F	5'CCCCAGTTCGAAAAGTAAGGACGCTCGAATTAGGCC3'
		110_Donor_RHDa6	5'AAATTTGTGTCGCCCTGAACTCGATTGCGCTGCTAGCTCATCTG3'
C-terminal tagging with FSVS-loxP-3Px3DsRED-loxP using as a template donors with FSVS tags above (fragments 31-33)			
nAChR subunit	fragment	site	oligonucleotides sequence
nAChR α 6	34	105_Donor_LHA_Da6	5'CGGGCTAATTATGGGGTGTGCCCTGTGCATGCAGAGAATGAAACC3'
		114_RHDa6_Tag_R	5'CTTTCGAACCTGGGGATGGCTCCAAGCTCC3'
	36	155_Marker_F1	5'CTTGGAGCCATCCCCAGTTCGAAAAGTAGTAAGGTACCGCGGGTATAAC3'
		157_Marker_R1	5'GGCTCTCTATATAACCTCGTATAGCATACTC3'
	36	165_Da6_F_marker	5'ATGCTATACGAAGTTATAGAAGAGCTAAGGACGCTCGAATTAGGCC3'
		110_Donor_RHDa6	5'AAATTTGTGTCGCCCTGAACTCGATTGCGCTGCTAGCTCATCTG 3'

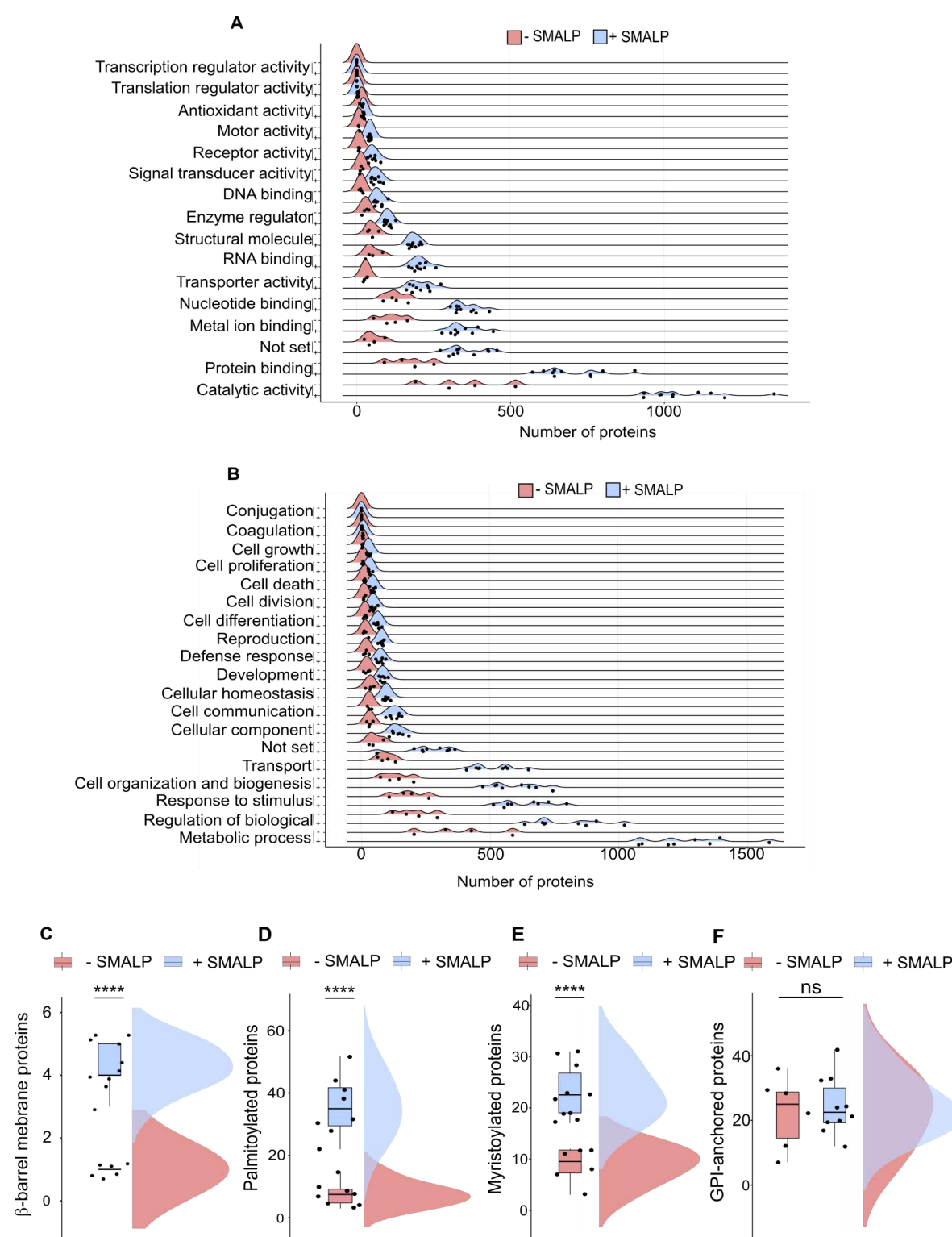


Figure supplement 1. GO terms and predicted membrane proteins.

(A) GO slim term for biological process and (B) for molecular function analysed within samples solubilized without or with SMA, n=4 or 11 per conditions. Predicted β -barrel membrane- (C), two-tailed t-test ****P<0.0001, n=6 or 10; palmitoylated- (D), ****P<0.0001, each n=8; myristoylated- (E), ****P<0.0001, n=6 or 10; and GPI-anchored proteins (F), non-significant ns, n=6 or 10.

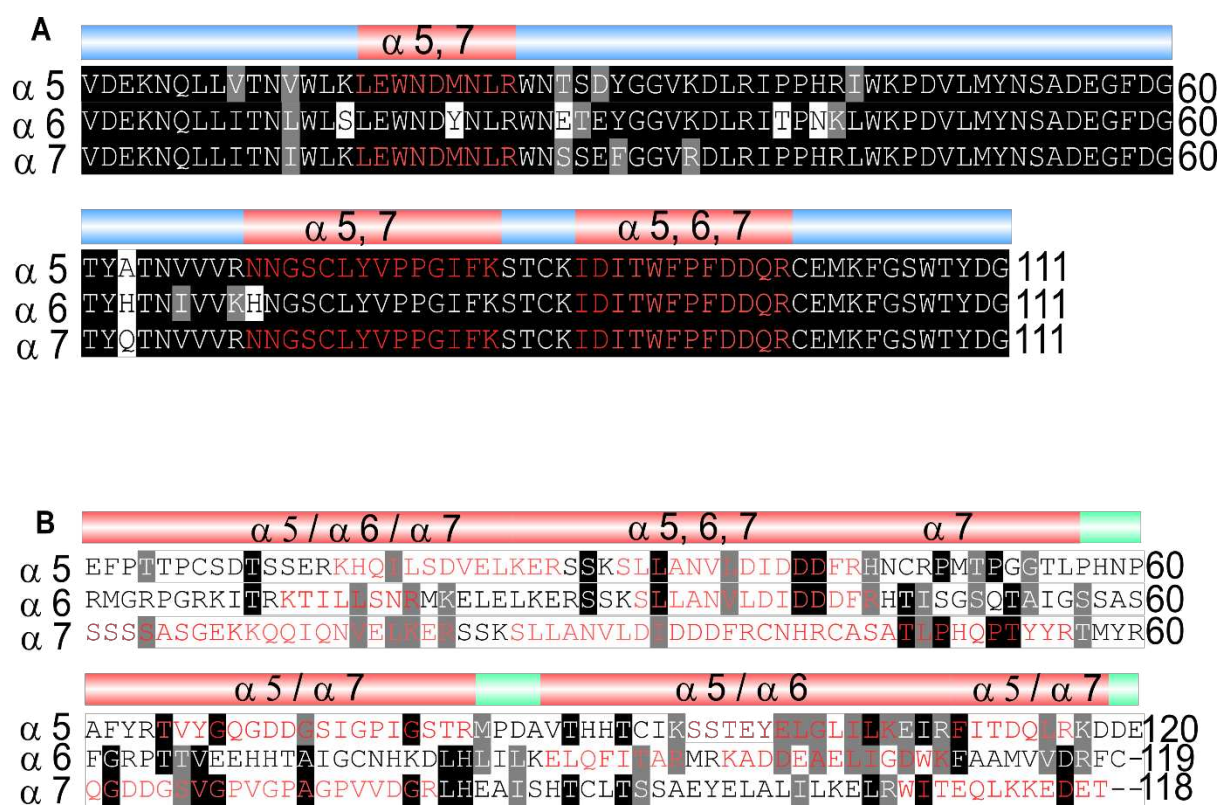


Figure supplement 2. Identified peptides in ligand-binding and cytoplasmic domain.

(A) Shared peptides found in the ligand-binding domains are shown in red. (B) Identified unique (/) and shared (,) peptides in cytoplasmic domains.

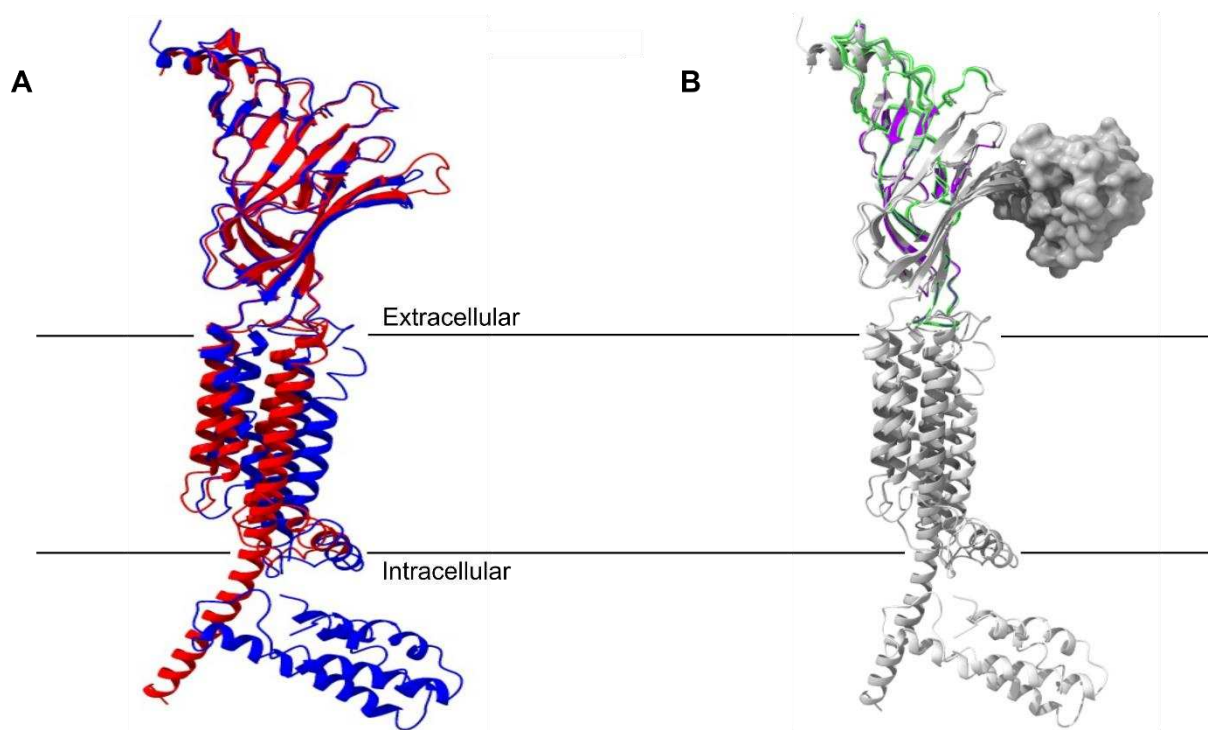


Figure supplement 3. Superimposed nAChR α -subunits structure together with identified peptides.

(A) Superimposed nAChR α -subunit structures from *Homo sapiens* (blue, PDB 6USF) and *Torpedo californica* (red, 6UWZ). Extracellular ligand-binding domain (LBD) illustrates a structure similarity.
(B) Same superimposed structures bound to α -bungarotoxin (α -Btx, surface structure). Peptides found in LBD are highlighted in green. The homology regions of D α 6 nAChRs LBD are shown in violet.

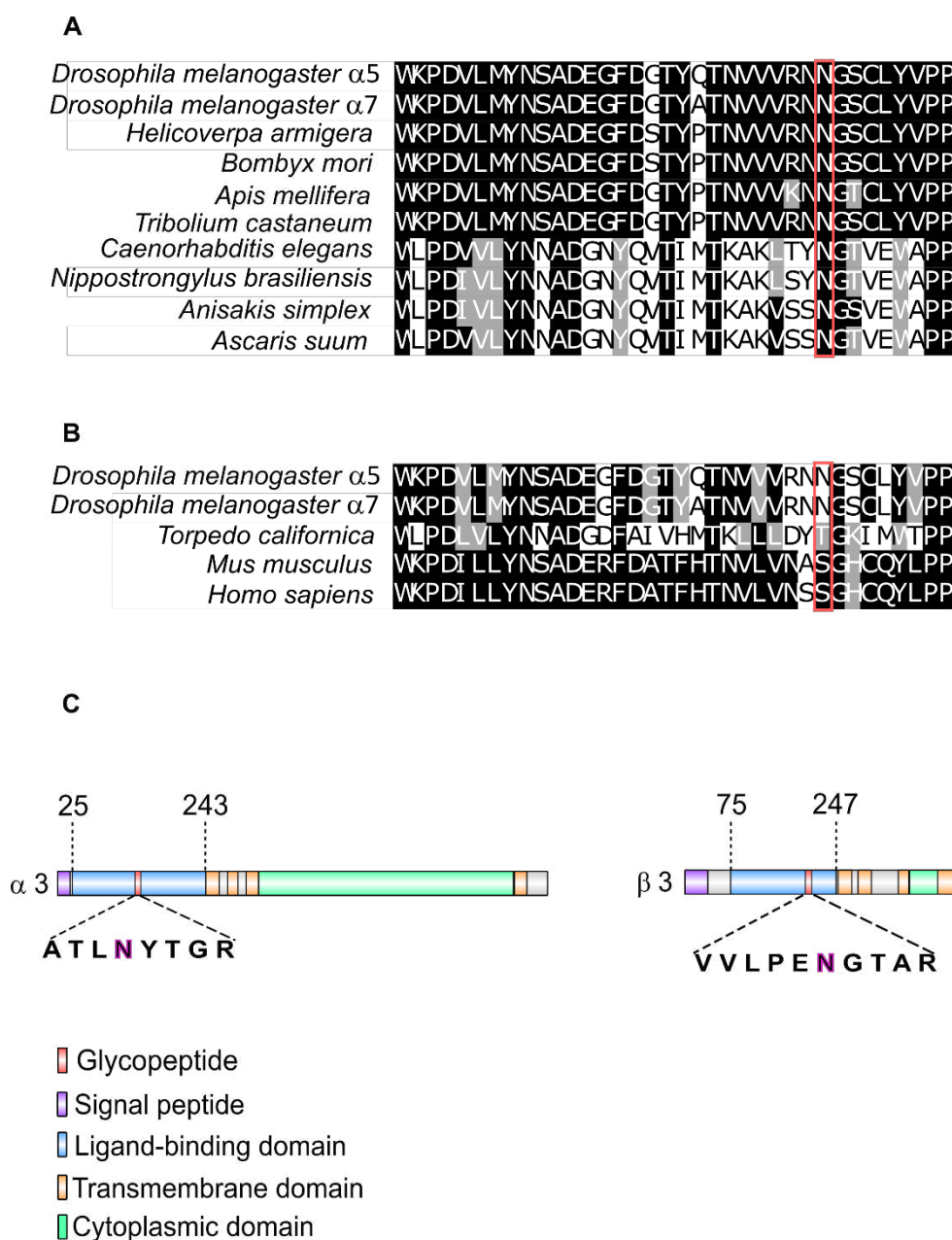


Figure supplement 4. Glycosylation sites of nAChR subunits.

(A) Multiple sequence alignment of insect $\alpha 7$ nAChR subunits compared to sequences of nematodes. The glycosylated ligand-binding domain (LBD) sequence of $\text{D}\alpha 5$ and $\text{D}\alpha 7$ nAChR subunits are shown. Glycosylated asparagine residues highlighted in red are conserved within insects and nematodes ($\text{D}\alpha 5$ 422 and $\text{D}\alpha 7$ 170 amino acids). **(B)** Same $\text{D}\alpha 5$ and $\text{D}\alpha 7$ nAChR subunit sequences compared to *T. californica*, *D. rerio*, *M. musculus* and *H. sapiens*. **(C)** Graphical representation of $\text{D}\alpha 3$ and $\text{D}\beta 3$ nAChR subunits. N-acetylhexosamine (H) modification on asparagine residues are highlighted and are of low site probability $\leq 80\%$.